科技部補助專題研究計畫成果報告
期末報告

具有缺氧標靶特性的光控藥物傳遞系統的開發與其在癌球幹細胞的偵測與治療上的應用

計 畫 類 別 ： 個別型計畫
計 畫 編 號 ： MOST 106-2113-M-040-001-
執 行 期 間 ： 106年08月01日至107年12月31日
執 行 單 位 ： 中山醫學大學醫學應用化學系(含碩士班)

計 畫 主 持 人： 朱智謙

計畫參與人員： 碩士班研究生-兼任助理：林彥成
碩士班研究生-兼任助理：黃棋榆
大專生-兼任助理：洪銘陽
大專生-兼任助理：邱彗舫
大專生-兼任助理：劉文璇

中 華 民 國 108 年 03 月 30 日

中 文 摘 要 ： 本年度計畫主要嘗試開發具有標靶缺氧特質的複合藥物傳遞與診斷系統。我們鎖定超過50%的癌細胞皆有過度表現的人類NQO1還原性酵素，開發出樹枝狀高分子衍生之螢光探針來分析此酵素在不同腫瘤細胞的表現狀態。針對腫瘤細胞內的生物還原性酵素表現，我們開發了以PAMAM 樹枝狀高分子為載體，外圍衍生香豆素的”turn-on”螢光探針複合系統。利用N=N 鍵來連結高分子載體與小分子探針，可以有效猝滅香豆素的強烈螢光，且從實驗結果證實，在電化學與化學還原的條件下，可以切斷N=N 鍵並釋放香豆素分子進而產生藍色螢光。從A549 與BT-474 兩種癌細胞株的螢光顯微影像分析中，我們也證實了樹枝狀高分子衍生之複合探針系統，可以有效區別二維細胞與三維癌球細胞內的NQO1 表現程度，而分析結果與利用NQO1 活性測定試驗法的結果相近，說明了三維A549 肺癌球細胞內的NQO1 表現量最高。癌球細胞通常被認為具有較多的癌症幹細胞特質，通常與癌症復發有顯著的關聯，因此我們將進一步透過分子設計導入抗癌藥物，讓此具有標靶癌球細胞內生物還原性酵素特性的樹枝狀高分子複合載體系統，能夠同時具備診斷與治療的效果。

中 文 關 鍵 詞 ： 香豆素、樹枝狀高分子、偶氮苯、藥物釋放、缺氧偵測、還原性酵素、癌症治療

英 文 摘 要 ： In this project, we aim to develop the hybrid delivery systems with hypoxia-targeting and detection ability. We focus on the human NQO1 reductase, which is usually over-expressed in solid tumors under hypoxia environment, and the PAMAM dendrimers are selected as the delivery vehicles for shuttling a novel coumarin-based fluorescence probes with “turn-on" sensing property. These probe molecules were covalently bonded at the dendrimer peripheral through an N=N linkage, by which blue fluorescence of coumain moieties can be effectively suppressed via a non-radiative relaxation. The intrinsic fluorescence is then completely recovered under electrochemical and chemical reduction because of the N=N bond cleavage. For A549 and BT-474 cancer cell lines, we introduced an epifluorescence microscope techniques to analyze the NQO1 levels in two-dimensional cells and three-dimensional tumorspheres using the hybrid probe system. The bioimaging analysis is consistent with the spectroscopic data determined by a conventional NQO1 activity assay method, indicating the A549 tumorspheres has the highest expression of the NQO1 reductase. Generally, the tumorspheres possess the property of cancer stem cells, which is highly correlated with cancer recurrence. Eventually, we will incorporate chemotherapeutic agents into the hybrid systems to achieve the tumor-targeting, detection, and treatment.

英 文 關 鍵 詞 ： Coumarins, dendrimers, azobenzenes, drug release, hypoxia detection, reductase, cancer therapy

期末報告

1. 前言

在固態腫瘤的增殖過程中，細胞內環境經常處於缺氧狀態(hypoxia)；由於細胞快速成長導致新生血管(neovascularisation)的缺陷，而不完整的血管網絡造成細胞內氧氣濃度偏低，因此讓生物還原性酵素(reductase)通常在缺氧的腫瘤細胞中大量表現[1,2]。目前具有標靶缺氧癌細胞特質的前驅藥物(prodrugs)則是化療藥物開發的重要方向之一，主要利用還原性酵素作用來驅動特定化學官能基的還原，進而讓藥物釋放出來達到標靶治療的效果。例如 evofosfamide 是一個目前已經進入第三期臨床試驗的抗胰臟癌與軟組織肉瘤的藥物，它具備可以被缺氧癌細胞中的 nitroreductase (NTR)還原的 2-nitroimidazole 基團，觸發後釋放出可嵌入 DNA 的交連劑分子，進而抑制腫瘤細胞的成長；而這些前驅藥物對於處於 normoxia 狀態的正常細胞組織則是無害的，因此具有標靶缺氧癌細胞的特性。另外，缺氧環境下大量表現的還原性酵素，也具有對抗活性氧物質 ROS 的能力，因此推測是化療抗藥性與癌細胞發生轉移(metastasis)的原因之一。

我們在本年度研究計畫中嘗試三個研究方向來開發具有標靶缺氧特質的複合型藥物傳遞與診斷系統。第一個是鎖定在 NCI-60 腫瘤細胞資料庫中，超過 50%的癌細胞皆有過度表現的人類 NAD(P)H:quinone oxidoreductase isozymes (NQO1)，開發出樹枝狀高分子衍生之螢光探針來分析 NQO1 還原性酵素在不同腫瘤細胞的表現狀態[3]；第二個則是標靶具有還原性酵素過度表現的粒線體，開發出咔唑-香豆素衍生之抗癌藥物傳遞系統，希望透過破壞不具有自動修復功能的粒線體 DNA，克服 chlorambucil 的抗藥性問題，進而提升抑制血癌細胞增殖的效果；第三個則是針對還原性酵素過度表現的人類結腸癌細胞，開發出寡胜肽側鏈修飾的褐藻酸高分子載體，提高蜂毒胜肽藥物 melittin 的治療效果。以下主要討論第一個主題的先期研究成果，第二與第三個研究主題已經準備投稿相關期刊，研究內容詳見附錄 II 與 III。

2. 結果與討論

NQO1 是一種伴隨輔酶 NAD(P)H 驅動的雙電子還原性酵素，可以有效還原醌(quinone)、硝基芳香烴(nitroaromatics)、偶氮(azo)等官能基，經常過度表現在缺氧狀態下成長的生物組織。而更重要的是，NQO1 的過度表現與腫瘤形成(tumorigenesis)及癌症幹細胞(cancer stem cells; CSC)有直接關聯，因此是前驅藥物標靶腫瘤細胞的重要因子之一。在先前的研究中，我們開發具有能量上轉換特性的奈米複合材料，我們利用鑭系摻雜的奈米晶體作為核心，並藉由層堆疊包覆法(layer-by-layer)將樹枝狀高分子固定在奈米粒子的表面，接著利用「樹枝狀高分子」來吸附光敏劑而得到光動力療法的複合材料[4]。由於此奈米晶體具有吸收近紅外光後上轉換為紫外光與可見光的能力，因此便可以讓此複合材料執行近紅外光驅動之光動力療法。這樣的策略對於具備三維結構的癌球狀細胞(tumorsphere)有極佳的深層治療效果。癌球細胞通常是在無血清的培養基質中以懸浮方式成長，且被認為具有較多的 CSC 特質，而 CSC 則與癌症復發有顯著的關聯，因此我們認為癌球細胞中的生物還原性酵素表現是一個值得探討的方向[5-7]。我們延續以 PAMAM 樹枝狀高分子作為功能性小分子載體(如光敏劑)，對於癌球細胞有較好的穿透效果的材料設計策略，以 7 號位置帶有推電子胺基的螢光香豆素 AMC 作為光敏感起始物，透過圖一的途徑合成出外圍以偶氮鍵(N=N)連結的香豆素衍生 G4-AzMC。偶氮鍵可以有效猝滅香豆素的藍色螢光，當 N=N 鍵被細胞內過度表現的 NQO1 還原並切斷後，釋放出香豆素分子讓螢光恢復成原有的狀態(屬於"turn-on"型的螢光探針)[8,9]。我們先利用 NMR 光譜分析來分析小分子探針在樹枝狀高分子外圍的取代率(degree of substitution; DS)，發現 DS 約為 6.1% (以 64 個外圍胺基來計算)；我們也利用偶氮苯分子 π-π*的特徵吸收峰，透過 UV-Vis 光譜分析來決定 DS 約為 5.9%。兩種分析結果相當接近，說明了平均每個 PAMAM 樹枝狀高分子衍生了約 4 個香豆素衍生之探針分子。另外，我們也由同樣的方法合成出控制組(negative control)，差別在於不攜帶香豆素分子，因此當 N=N 鍵被還原後不會產生螢光"turn-on"的現象。

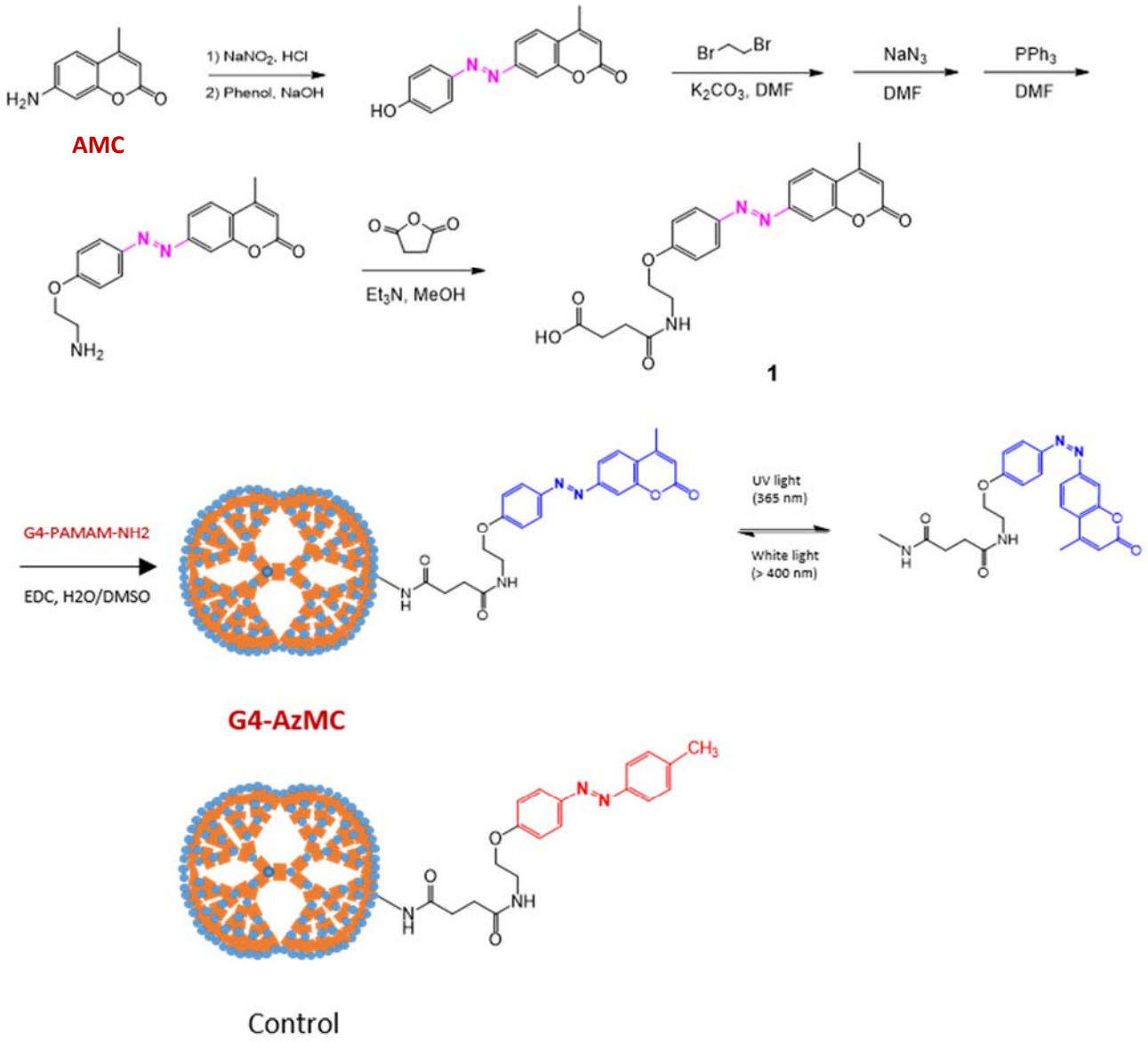

圖 1. 攜帶香豆素螢光探針的 PAMAM 樹枝狀高分子 G4-AzMC 的合成途徑示意圖。

圖二 A 為 G4-AzMC 的吸收光譜圖，在暗室中呈現 380-nm 的 π-π*特徵吸收峰，相較於 7 號胺基取代之香豆素起始物在 340-nm 左右的最大吸收峰，紅位移了約 40-nm，證明了 N=N 鍵有效延伸了共軛系統長度。由於偶氮苯具有光致順反異構化的特性，因此在照射 365-nm 的 UV 光後，反式結構轉變成順式結構(如圖一所示)，因此原本 π-π*吸收波長消失；而在照射白光後又再度上升。如圖二 B 所示，透過照射 UV 光與白光的切換可以誘導可逆的順反異構化反應，上述結果證實了 PAMAM 樹枝狀高分子外圍成功衍生了以 N=N 鍵連結的香豆素探針分子。

圖二 C 與 D 分別為探針分子 **1** 與 G4-AzMC 的循環伏安法的掃描圖譜，可以明顯發現 **1** 在-0.71 與-1.79V 的兩個不可逆的還原電位，符合文獻中所述之 N=N 鍵的還原與斷裂時，至少需要兩顆電子的作用。NQO1 為雙電子還原性酵素，預期也可以在輔酶 NAD(P)H 的作用下切斷 N=N 鍵。而在+1.28 與+1.77V 兩個不可逆的氧化電位，推測為香豆素分子的氧化作用。由於 G4-AzMC 只能溶解在水溶液中，受限於掃描範圍只能在-0.52V 與+0.91V，分別觀察到還原與氧化電位，證明樹枝狀高分子衍生之探針分子同樣具有氧化還原能力。

圖二 E 為 G4-AzMC 的螢光光譜分析，在 380-nm 光激發下螢光非常微弱，證實了 N=N 官能基有效猝滅了香豆素原本強烈的螢光(螢光量子效率約 0.5)；當我們以 $Na_2S_2O_4$ 進行化學還

原反應後，恢復最大放射波長約為 450-nm 的藍色螢光。圖二 F 為還原處理後的 G4-AzMC 吸收光譜分析，最大吸收波長與原本的香豆素起始物相吻合(340-nm)，而在反覆照射 UV 光與白光都不會觀察到吸收度的變化，代表化學還原法切斷了 N=N 鍵結，因此失去光致順反異構化的能力。如圖二 G 所示，在還原條件下可以讓香豆素探針從樹枝狀高分子載體上釋放出來，恢復原本的藍色螢光強度而達到"turn-on"偵測的效果。

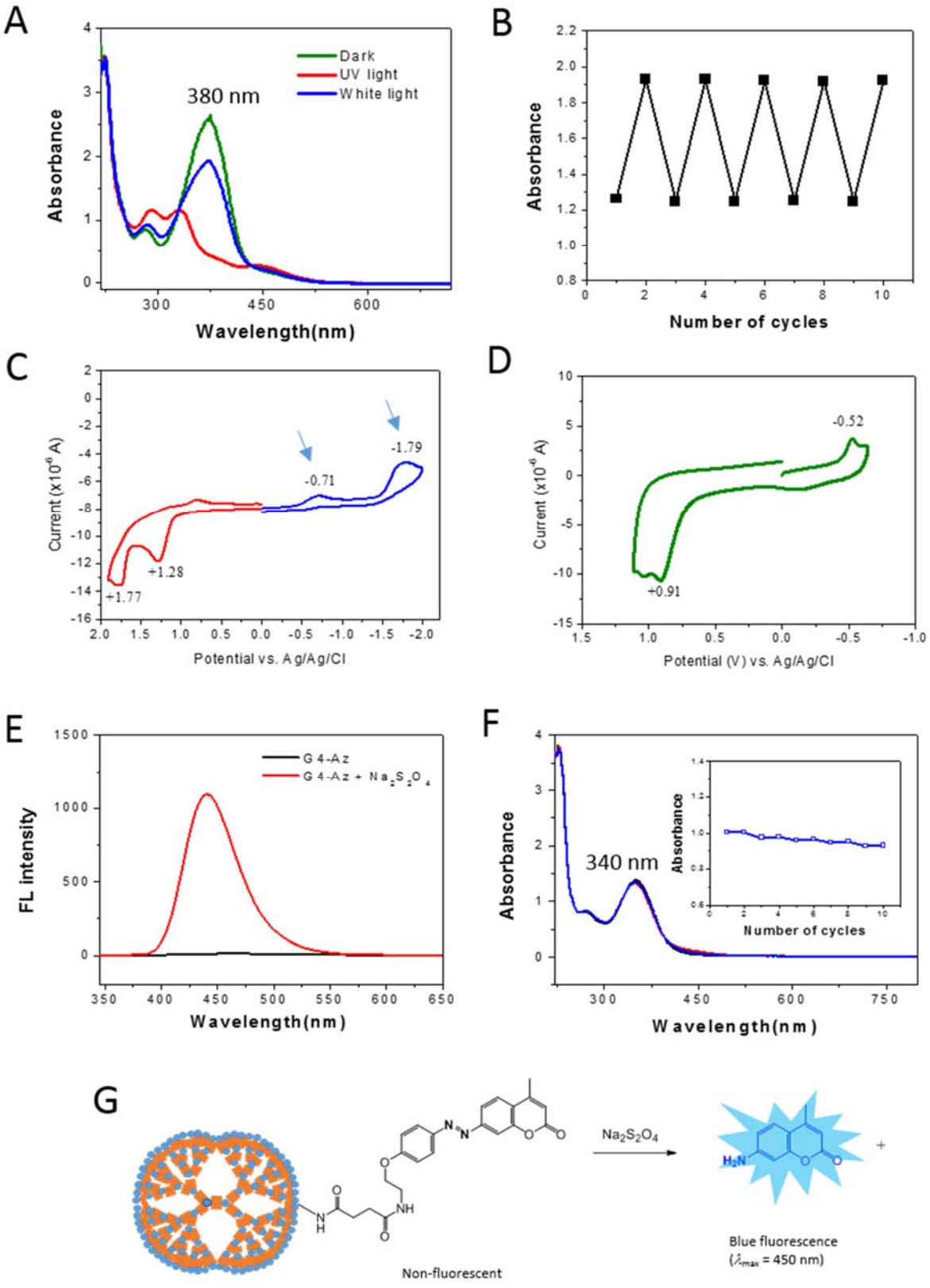

圖 2. (A) G4-AzMC 的 UV-Vis 吸收光譜分析，照射之 UV 光波長為 365-nm，白光為一般市售的燈泡，波長>400-nm。(B) 以 UV 與白光替換照射所誘導之可逆光致順反異構化行為。(C) 化合物 **1** 在 CH_3CN 中的 CV 掃描圖譜。(D) G4-AzMC 在水中的 CV 掃描圖譜。(E) G4-AzMC 以 $Na_2S_2O_4$ 還原處理後的螢光光譜分析。(F) G4-AzMC 以 $Na_2S_2O_4$ 還原處理後的 UV-Vis 吸收光譜分析，UV 與白光替換照不會產生吸收度與波長的變化。(G) G4-AzMC 的化學還原反應與釋放螢光香豆素分子示意圖。

證明 G4-AzMC 在電化學與化學方法下被還原，並且能夠順利釋放螢光香豆素探針後，我們接著嘗試將材料導入 NQO1 過度表現的腫瘤細胞中。首先利用 NQO1 活性測定法來分析二維培養癌細胞株與三維癌球細胞的差異。該測定法的分析原理是利用 menadione 作為活性物質，並以輔酶 NADH 作為電子提供者，觸發 NQO1 的酵素還原反應得到 hydroquinone，反應同時也讓 WST-1 氧化得到在 440-nm 有顯著吸收的 formazan，間接透過此顯色反應來決定酵素的活性表現。如圖三 A 所示，我們利用人類 NQO1 重組蛋白質作為對照組(活性≥0.1U)，來分析二維與癌球 A549 肺腺癌細胞與 BT-474 乳癌細胞，其等蛋白濃度的細胞裂解物(cell lysate)的 NQO1 活性表現。由結果發現 NQO1 在三維癌球細胞中的活性較二維細胞株高，且 A549 細胞株的酵素表現也比 BT-474 細胞株高 [10]；另外，我們也嘗試利用此測定法來分析 G4-AzMC 對於 NQO1 的反應活性，從圖三 B 可以發現隨著反應時間的增加，formazan 在 440-nm 的吸收度逐漸上升，說明了以 G4-AzMC 作為活性觸發物的效率與 menadione 標準品相近(positive control)，也間接證實 NQO1 可以有效還原樹枝狀高分子外圍的 N=N 鍵結，並可能釋放出香豆素探針分子。

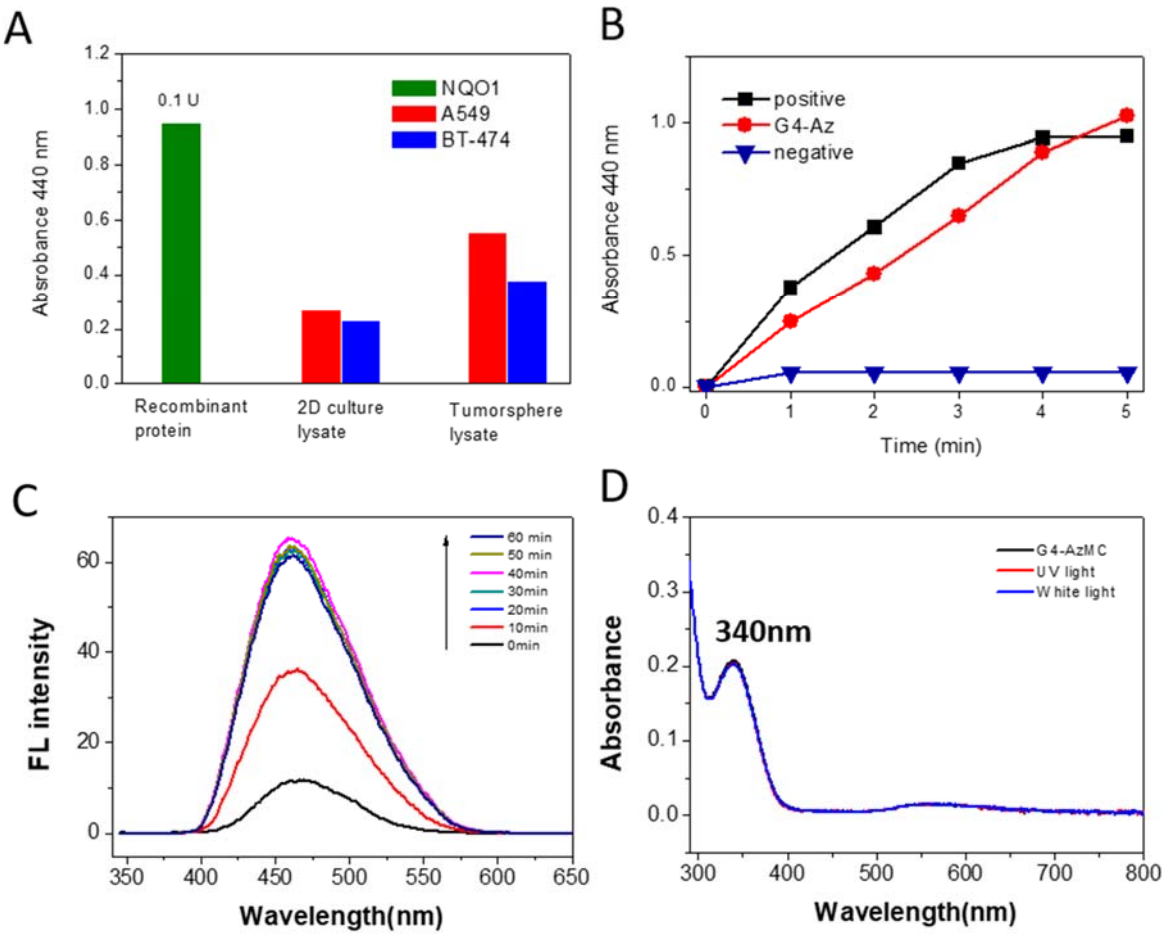

圖 3. (A) NQO1 活性測定分析結果，A549 與 BT-474 分別為肺腺癌細胞與乳癌細胞株。測定物質為二維細胞與三維癌球細胞裂解物。(B) 以 NQO1 活性測定來分析以 G4-AzMC 為活性物質的酵素還原效果，positive 與 negative 控制組分別為使用 menadione 與 dicoumarol 為活性物質。(C) G4-AzMC 在 NQO1 與β-NADH 還原處理後的螢光光譜分析。(D) G4-AzMC 在 NQO1 與β-NADH 還原處理後的 UV-Vis 吸收光譜分析，UV 與白光替換照並不會產生吸收度與波長的變化。

圖三 C 為 G4-AzMC 的螢光強度隨著加入 NQO1 後逐漸上升並飽和的趨勢，說明了當 N=N 鍵結被還原切斷後，可以順利釋放出香豆素分子並產生明顯的藍色螢光；圖三 D 為與 NQO1 反映後的 G4-AzMC 的吸收光譜分析，位於 340-nm 左右的吸收峰並不會受到 UV 與白光的刺激而產生吸收度的變化，此結果吻合化學還原法處理後的 G4-AzMC，代表化學還原法切斷了 N=N 鍵結，而釋放出來的 AMC 香豆素探針並不具有光致順反異構化的能力。

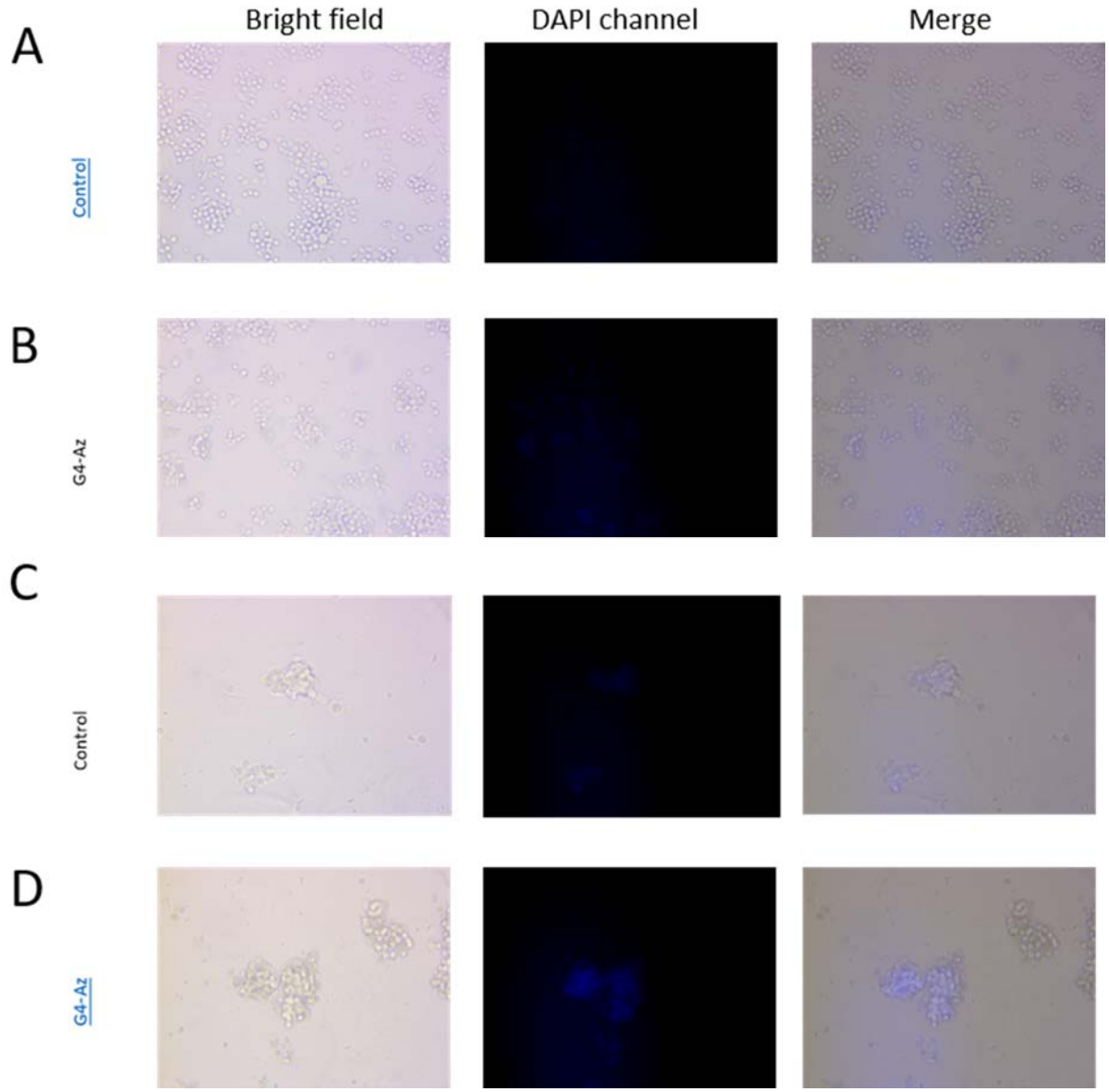

圖 4. 光學顯微鏡亮視野與 DAPI-channel 螢光通道與重疊影像分析: (A) 以 control 組處理之二維 BT-474 乳癌細胞。(B) 以 G4-AzMC 處理之二維 BT-474 乳癌細胞。(C) 以 control 組處理之三維 BT-474 乳癌球細胞。(D) 以 G4-AzMC 處理之三維 BT-474 乳癌球細胞。

最後我們嘗試利用 G4-AzMC 與不攜帶香豆素探針的樹枝狀高分子衍生物作為 control 組(圖一)，搭配螢光顯微技術直接分析兩種腫瘤細胞株在二維與三為狀態下的還原性酵素表現。圖四 A 與 B 分別為對照組與 G4-AzMC 在二維培養之 BT-474 細胞株的在亮視野與 DAPI-channel 螢光通道的生物影像分析，結果顯示以 G4-AzMC 處理後的細胞株，具有較明顯的藍色螢光表現；圖四 C 與 D 則為三維癌球細胞在兩種樹枝狀高分子衍生物處理後的影像分析，可以發現以 G4-AzMC 處理後的癌球細胞株之藍色螢光最為明顯。此結果與 NQO1 活性分析數據相吻合，都說明了癌球細胞具有較高的還原性酵素表現，因此所釋放出來的香豆素探針所產生的螢光也較強。而控制組因為外圍不具有香豆素分子，因此所呈現出來的微弱藍色螢光就是背景值了。

圖五為同樣以樹枝狀高分子衍生物處理之 A549 癌球細胞株的螢光影像分析，結果與 BT-474 細胞株的影像分析相似，以 G4-AzMC 處理後的癌球細胞株具有非常明顯的藍色螢光表現，而控制組只呈現出微弱的螢光背景值。值得注意的是處理後的 A549 癌球細胞所展現的螢光強度比 BT-474 癌球細胞來得明顯，這也吻合 NQO1 活性測定細胞裂解物的分析結果，說明了 A549 三維癌球細胞具有最高的酵素活性表現，而我們所設計出來的 G4-AzMC 螢光探針也可以達到同樣的分析效果。若能進一步透過流式細胞儀來分析這些細胞株的螢光表現，就可以得到酵素活性分析的量化分析數據了[11]。

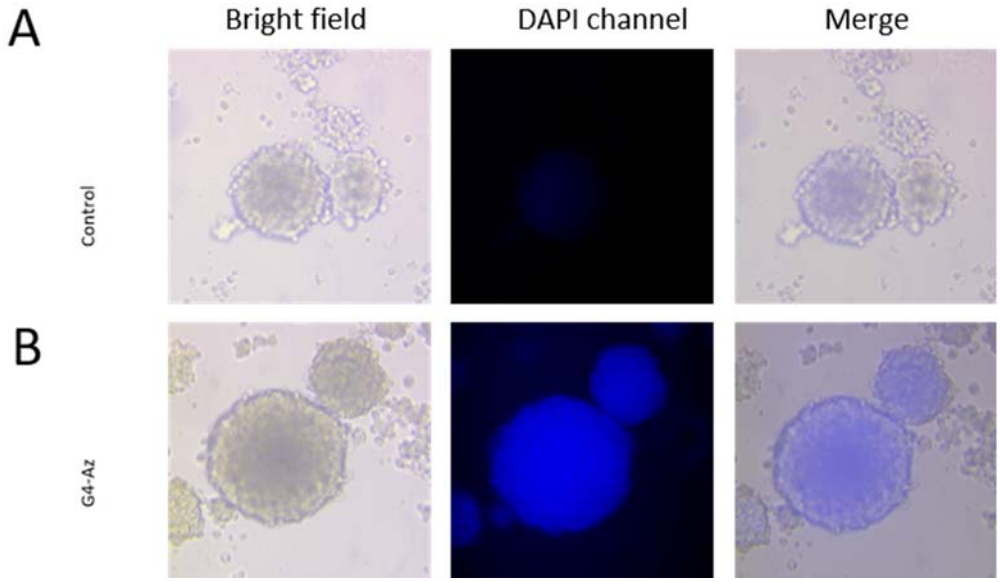

圖 5. (A) 光學顯微鏡亮視野、DAPI-channel 螢光通道與重疊影像分析: (A) 以 control 組處理之三維 A549 肺腺癌球細胞。(B) 以 G4-AzMC 處理之三維 A549 肺腺癌球細胞。

3. 結論

針對腫瘤細胞內的生物還原性酵素表現，我們開發了以 PAMAM 樹枝狀高分子為載體，外圍衍生 AMC 香豆素的"turn-on"螢光探針複合系統。利用 N=N 鍵來連結高分子載體與小分子探針，可以有效猝滅 AMC 香豆素的強烈螢光，且從實驗結果證實，在電化學與化學還原的條件下，可以切斷 N=N 鍵並釋放香豆素分子進而產生藍色螢光。從 A549 與 BT-474 兩種癌細胞株的螢光顯微影像分析中，我們也證實了樹枝狀高分子衍生之複合探針系統，可以有效區別二維細胞與三維癌球細胞內的 NQO1 表現程度，而分析結果與利用 NQO1 活性測定試驗法的結果相近，說明了三維 A549 肺癌球細胞內的 NQO1 表現量最高。癌球細胞通常被認為具有較多的癌症幹細胞(CSC)特質，而 CSC 則與癌症復發有顯著的關聯，因此我們將進一步透過分子設計導入抗癌藥物，讓此具有標靶癌球細胞內生物還原性酵素特性的樹枝狀高分子複合載體系統，

能夠同時具備診斷與治療的效果。

4. 參考文獻

(1) Denny, W. A. *The Lancet Oncol.* **2000**, *1*, 25.

(2) Carnero, A.; Lleonart, M. *Inside the Cell* **2016**, *1*, 96.

(3) Oh, E.-T.; Park, H. J. *BMB Reports* **2015**, *48*, 609.

(4) Wang, B.-Y.; Liao, M.-L.; Hong, G.-C.; Chang, W.-W.; Chu, C.-C. *Nanomaterials* **2017**, *7*, 269.

(5) Chen, Y.-C.; Lou, X.; Zhang, Z.; Ingram, P.; Yoon, E. *Sci. Rep.* **2015**, *5*, 12175.

(6) Lee, C.-H.; Yu, C.-C.; Wang, B.-Y.; Chang, W.-W. *Oncotarget* **2015**, *7*, 1215.

(7) Weiswald, L.-B.; Bellet, D.; Dangles-Marie, V. *Neoplasia* **2015**, *17*, 1.

(8) Piao, W.; Tsuda, S.; Tanaka, Y.; Maeda, S.; Liu, F.; Takahashi, S.; Kushida, Y.; Komatsu, T.; Ueno, T.; Terai, T.; Nakazawa, T.; Uchiyama, M.; Morokuma, K.; Nagano, T.; Hanaoka, K. *Angew. Chem. Int. Ed.* **2013**, *52*, 13028.

(9) Sharma, R.; Rawal, R. K.; Gaba, T.; Singla, N.; Malhotra, M.; Matharoo, S.; Bhardwaj, T. R. *Bioorg. Med. Chem. Lett.* **2013**, *23*, 5332.

(10) Shen, Z.; Prasai, B.; Nakamura, Y.; Kobayashi, H.; Jackson, M. S.; McCarley, R. L. *ACS Chem. Biol.* **2017**, *12*, 1121.

(11) Elmes, R. B. P. *Chem. Commun.* **2016**, *52*, 8935.

附錄 I

Full Paper

Targeted photoresponsive carbazole-coumarin nanoconjugates for efficient combination therapy in Leukemia cancer cells

Bing-Yen Wang,[a] Yen-Cheng Lin,[b] Yi-Ting Lai,[c] Wen-Wei Chang,*[c] and Chih-Chien Chu,*[bd]

[a]Division of Thoracic Surgery, Department of Surgery, Changhua Christian Hospital, Changhua, Taiwan
[b]Department of Medical Applied Chemistry, Chung Shan Medical University, Taichung, Taiwan
[c]Department of Biomedical Science, Chung Shan Medical University, Taichung, Taiwan
[d]Department of Medical Education, Chung Shan Medical University Hospital, Taichung, Taiwan

*Corresponding Author: Chih-Chien Chu

Department of Medical Applied Chemistry

Chung Shan Medical University

No. 110, Sec. 1, Jianguo N. Rd., Taichung 40201, Taiwan

TEL/FAX: +886-4-2324-8189; E-mail: **jrchu@csmu.edu.tw**

Introduction

Photo-triggered drug delivery systems (PTDDS) have aroused much attention because light stimulation provides excellent spatial and temporal control over the photoactive nanocarriers to release loaded drugs under an active pathway.[1] Moreover, light can be externally applied and easily tuned to a desired wavelength and power toward versatile therapeutic purposes.[2] Generally, a PTDDS possesses a tailor-made chemical structure composed of a drug molecule caged with a photolabile building block and targeting ligands. After reaching the designated position, the PTDDS is accumulated topically in a dormant state until light stimulation is activated. The drugs can thus be photocontrolled release to achieve the chemotherapeutic outcome. Accordingly, the photolabile chromophores that are responsive to UV, visible, and near-infrared (NIR) light are crucial to the development of an effective PTDDS.

Among the synthetic phototriggers with well-established photolytic mechanisms, coumarin-based derivatives that undergo efficient photolysis exhibit some unique features such as efficient fluorescence visualization and tunable absorption wavelength.[3] The photolysis involving facile C-O bond cleavage upon light irradiation simply produces a free drug and solvent-trapped coumarin as the photo by-product.[4] Moreover, coumarin substituted at 7-poisiotn with an electron-donating group are known to exhibit red-shifted absorption and emission wavelength at blue-green light region. For example, 7-aminocoumarins with remarkable fluorescence quantum yield have been used as optical brighteners, fluorescent probes, and phototriggers.[5] Lin et al. have reported effective photorelease of anticancer drugs regulated by either a one- or two-photon excitation process, combining the intrinsic fluorescence of the coumarin for tracing biodistribution makes these coumarin-based materials would be a favored PTDDS candidate toward biomedical applications.[6]

In this paper, we introduce a carbazole-coumarin (CC) fused heterocycle as the PTDDS platform for performing photocontrolled release of anticancer drugs.[7] Because the amine moiety of the carbazole may serve as an electron donor and the lactone moiety of the coumarin may act as an electron acceptor, the coumarin building block with a “push-pull” nature undergoes a photolytic reaction under more extended wavelengths to visible light. Zheng et al. have reported that the CC derivatives possess one- and two-photon fluorescence probe for imaging carbon monoxide in living tissues.[8] By exploiting the photocontrolled release and other unique features, we focus on the development of robust synthetic routes for preparing the CC-drug conjugates. Herein, we use a historical nitrogen mustard, chlorambucil, as the drug linkage in chemotherapeutic regimens. Moreover, the secondary amine group on the carbazole ring also permits a facile chemical modification of a site–specific targeting ligand, driving the conjugate system more effective in cancer treatment.

1. Results and discussion

2.1 Synthesis of the CC-drug conjugates.

A commercial available 4-hydroxycarbazole was selected as the starting material for constructing the carbazole and coumarin fused heterocycles. As shown in Figure 1a, the first step for the formation of **CC-1** involves a Lewis acid-catalyzed Pechmann condensation using ethyl acetoacetate for the lactone synthesis; after methylation of the amine in the carbazole ring to give **CC-2**, the allylic group in the coumarin ring was further oxidized by SeO_2, followed by subsequent reduction with $NaBH_4$ to yield **CC-3** with a significant allyl alcohol, which allows for the conjugation of the anticancer drug "chlorambucil" through a DCC-promoted esterification. However, the overall yield for the three steps is less than 10%, and the low yield is mainly due to the lower solubility of **CC-2** in organic solvents during the heterogeneous oxidation process.

Alternatively, as shown in Figure 1b, we developed a synthetic route based on a modified condensation reaction using ethyl 4-chloroacetoacetate for the coumarin formation. The **CC-4** bearing an electrophilic allyl chloride was thus prepared under the catalysis of methanesulfonic acid. To increase the solubility in solvents, the amine in the carbazole was reacted with excess *tert*-butyl bromoacetate in the presence of K_2CO_3 to yield **CC-5** functionalized with an acid-labile *tert*-butyl ester (OtBu) group. However, hydrolyzing the allyl chloride of **CC-5** in acetone/water (1:1) mixture was failure to give an alcohol group. We assumed that the nucleophilic substitution in a protic solvent tends to the formation of carbocation in the allylic position, thus leading to undesired intramolecular side reactions in the CC ring rather than intermolecular nucleophilic attack by H_2O. A stronger nucleophile and aprotic media are crucial for performing the substitution reaction. Accordingly, the chlorambucil drug was first treated with K_2CO_3 to possess a carboxylate ion as a stronger nucleophile, and then subsequent substitution with **CC-5** was successfully carried out in a DMF solution to yield the OtBu-protected **CC-6**. Comparing with the first pathway, this route with an overall yield of approximately 40% takes less synthetic steps, providing an efficient and robust method for the construction of the CC-drug conjugates, especially the drug containing COOH groups. Notably, the OtBu group can be quantitatively removed in acidic environment, and the final **CC-7** bearing an additional COOH group derived from the amine group in carbazole allows for further chemical modification. Moreover, the **CC-7** exhibits much better solubility in polar solvents, suchlike DMSO that is commonly used as a co-solvent with H_2O in biomedicinal experiments.

As shown in Figure 1c, to further increase the antiproliferative activity of the CC-drug conjugates, we introduce a triphenylphosphonium (TPP) group into the carbazole ring to yield **CC-8** through a facile amide-coupling reaction.[9] The TPP group possessing a delocalized cationic property has been proven as an efficient mitochondria-targeting ligand. It has been reported that the TPP is accumulated 5- to 10-fold into the cytoplasm from the extracellular space by the plasma membrane potential ($\Delta\psi_p$

= -30 to -60 mV) and then further accumulated 100- to 500-fold into the mitochondria matrix by the mitochondria membrane potential ($\Delta\psi_m$ = -150 to -170 mV).[10] Accordingly, the cellular uptake efficiency for conjugates could be enhanced, and then the photo-triggered released species is capable of damaging mitochondrial DNA (mtDNA), thus leading to mitochondria dysfunction and eventually cell death.

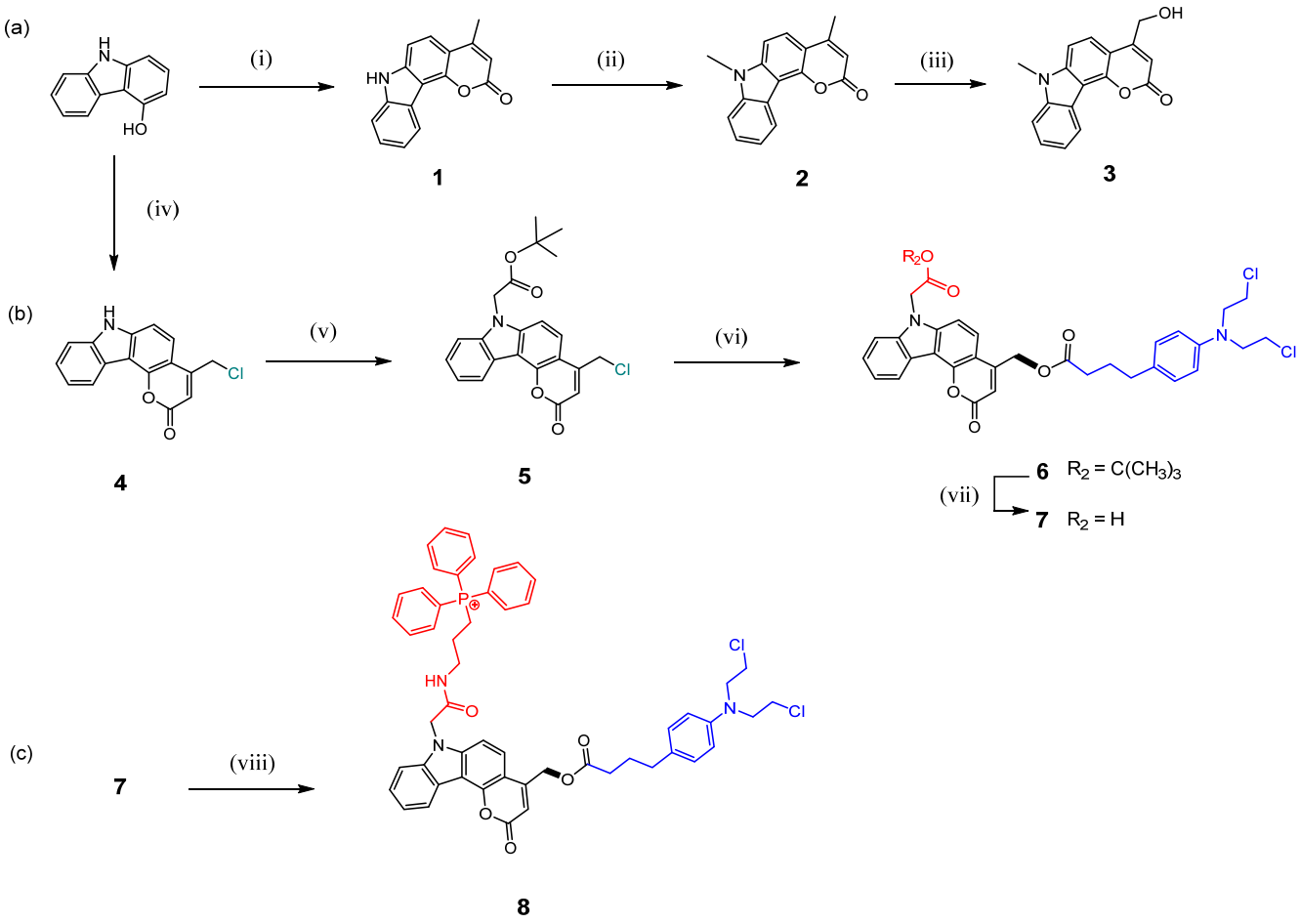

Figure 1. Synthesis of carbazole-coumarin (**CC**) derivatives **1**-**8**. Conditions: (i) ethyl acetoacetate, $ZnCl_2$, EtOH; (ii) CH_3I, K_2CO_3, DMF; (iii) SeO_2, PhMe; (iv) ethyl 4-chloroacetoacetate, CH_3SO_3H; (v) *tert*-butyl bromoacetate, K_2CO_3, DMF; (vi) chlorambucil, K_2CO_3, DMF; (vii) CF_3COOH; (viii) (3-aminopropyl)triphenylphosphonium bromide, HATU, Hünig's base, DMF.

2.2 Visible-light-triggered photorelease for CC-drug conjugate

Based on the fused heterocyclic structure, **CC-7** and **CC-8** dissolved in methanol solutions exhibits π-π* absorption and emission bands centered at approximately 360-nm and 450-nm, respectively (Figure 2). According to the photo-S_N1 cleavage mechanism, photochemical reaction and fluorescence represent the two main deactivation pathways of the first singlet excite state (S_1).[4, 11] Therefore, the photo-labile C-O bond that interconnects the CC moiety with a chlorambucil drug can be simultaneously cleaved in a protic solvent (e.g., methanol, H_2O) when the **CC** derivatives perform a photoluminescent process. Moreover, this photolytic liberation is usually combined with a marked fluorescence enhancement and can be thus monitored by fluorescence measurements. Notably, although the **CC** derivatives possess an absorption maximum located at UV region, weak absorption tail toward the wavelengths longer than 400-nm allows for visible-light-triggered photocleavage, which may cause less damage to biological specimen.

As shown in Figure 2a and 2b, UV-vis and fluorescence spectra display the time-dependent profile upon irradiation of 405-nm laser diode (LD). After light exposure, the absorption and emission profiles are still centered at the same wavelengths for the non-irradiated samples, but the change in absorbance and fluorescence intensity shows a reverse course; the emission intensity was dramatically increased as the absorbance was slightly decreased during light irradiation for 10 min. Notably, the **CC-8** possesses much stronger fluorescence enhancement than **CC-7** upon light excitation at the same concentration ($1x10^{-4}$ M). When we further examined fluorescence quantum yields (QY) for the dilute solutions of **CC** derivatives ($1x10^{-5}$ M), however, two fluorescence QY values were comparable (approximately 0.19 for **CC-7** and 0.21 for **CC-8**) with respect to a photoluminescence reference of 9,10-diphenylanthrance.[12] After light excitation, the QY values for **CC-7** and **CC-8** are increased to approximately 0.3. Comparing the solutions with different concentrations, we assumed that the **CC-7** may undergo self-aggregation in polar solvents under light exposure and thus leads to severe self-quenching fluorescence behavior at relatively higher concentration; in contrast, the TPP moiety grafted on the **CC-8** could assist with better dispersive ability in both polar and nonpolar solvents, thus preventing molecular aggregation and self-quenching process. According to the previous study, the fluorescence increment is combined with the photolytic reaction of the coumarin-derived photocages, and the marked fluorescence enhancement during photocleavege is definitely an extra bonus for the visualization of the photolytic process and drug release inside living cells.[4]

The photoinduced release of chlorambucil drugs was characterized by a reverse-phase HPLC analysis. As shown in Figure 3a, the **CC-7** and chlorambucil were identified as the elution peaks at 3.5 and 3.9 min, respectively. The amount of **CC-7** continuously drops combined with gradual accumulation of the free drugs in the solution as the irradiation time of 405-nm LD increases. Moreover, the drug released from the **CC-8** was eluted at 5.1 min and accumulated after light trigger.

The results conclude that the visible-light-triggered photocleavage efficiently produces the anticancer drugs in the two systems. Figure 3b shows the correlations of the laser irradiation time and released drug concentrations calculated from the peak areas relative to a chlorambucil standard solution. The free drug was successively accumulated until reaching a maximum value of approximately 50 μM for **CC-7** and 30 μM for **CC-8** after irradiating for 20 min. Figure 3c illustrates this photolytic process that the C-O linkage was cleaved in protic polar solvents under light excitation, and one chlorambucil molecule was then released from one **CC**-drug conjugate. Taking all data into account, the spectroscopy and HPLC analysis confirm that the visible light with 405-nm wavelength is sufficient to drive this photochemical reaction.

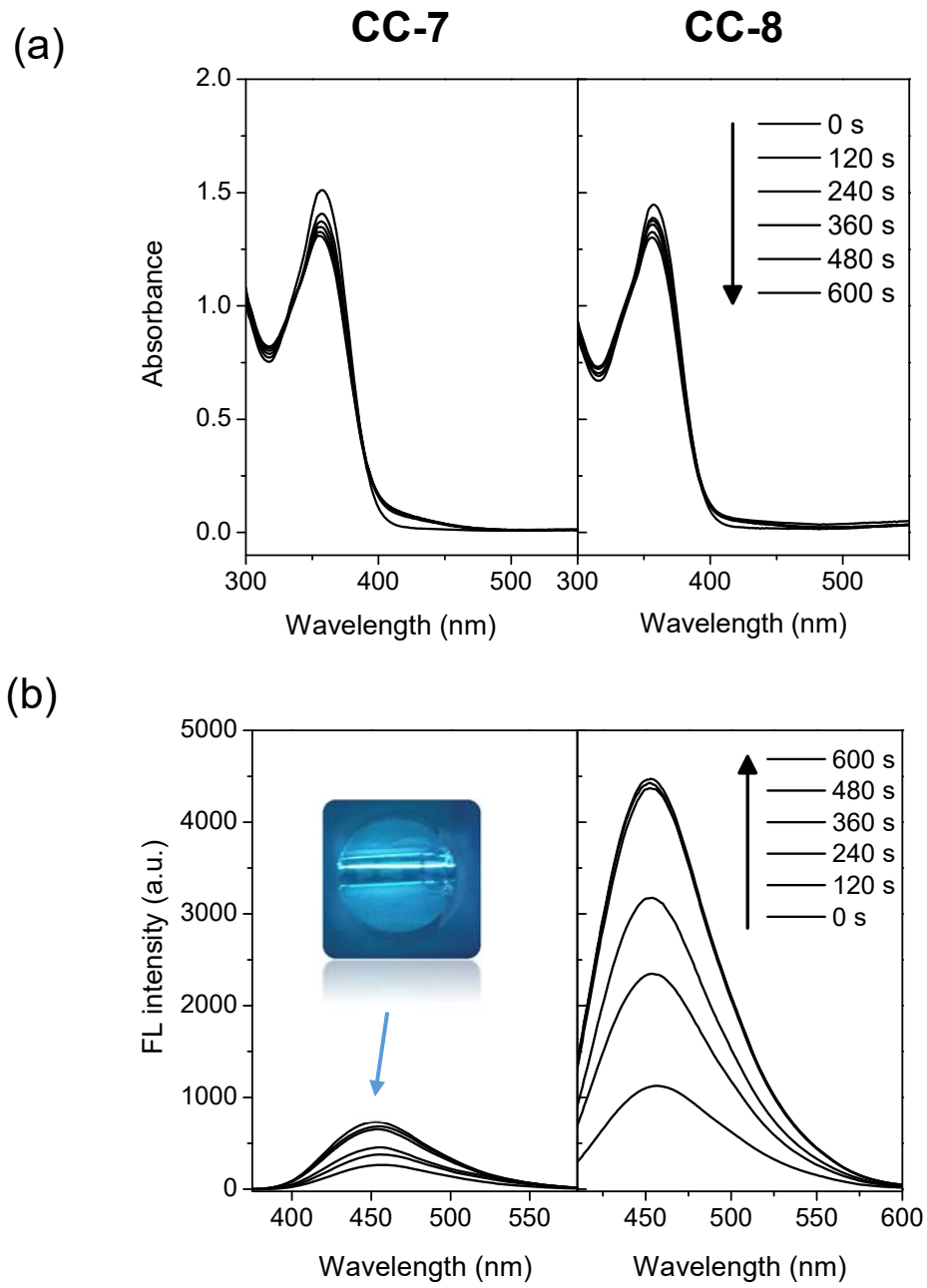

Figure 2. (a) UV-vis and (b) fluorescence spectra of **CC-7** and **CC-8** upon 405-nm laser irradiation (0-10 min). The absorption λ_{max} for **CC-7** and **CC-8** is 360-nm; fluorescence quantum yields for **CC-7** and **CC-8** are 0.19 and 0.21, respectively with respect to 9,10-diphenylanthrance standard.

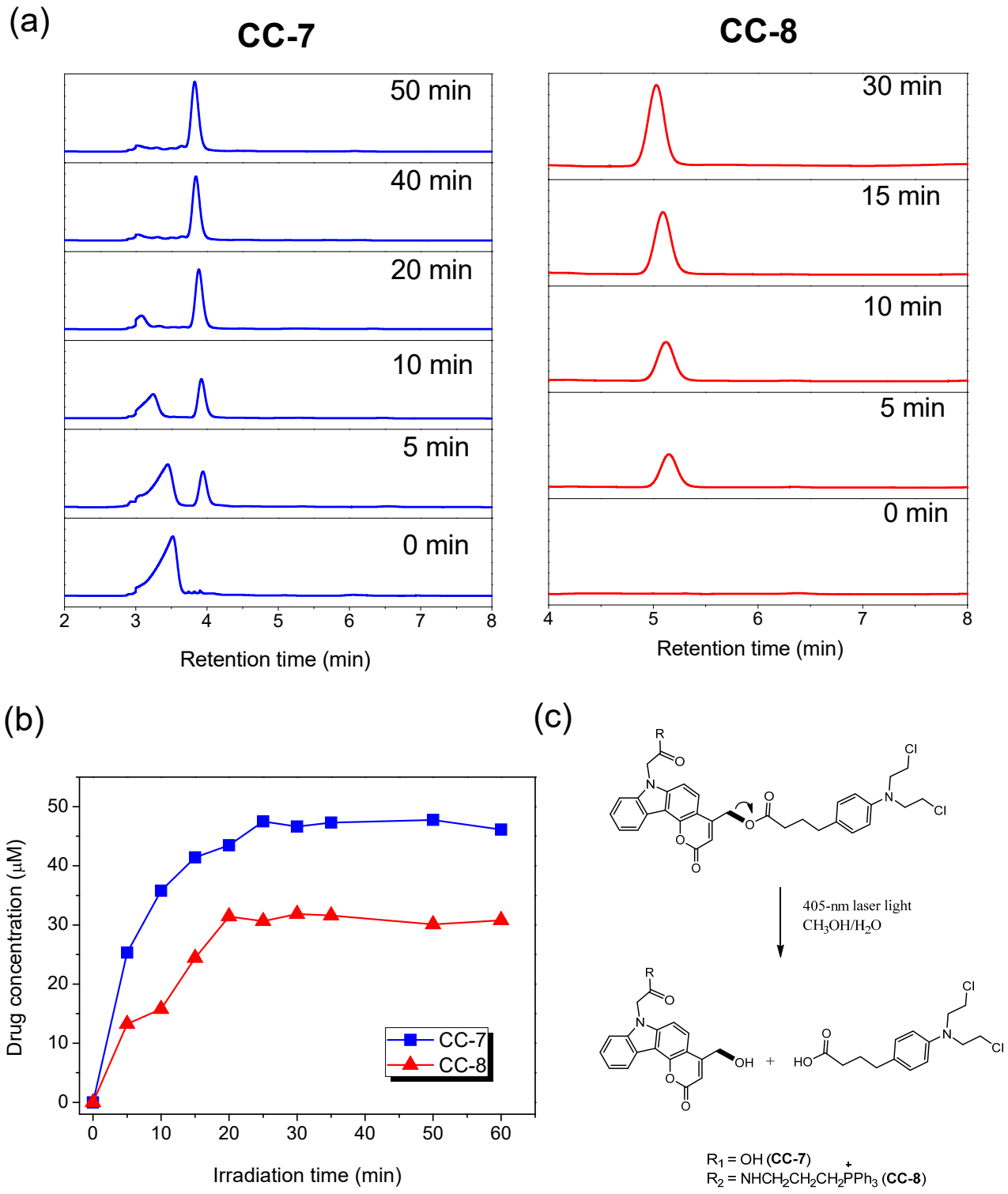

Figure 3. (a) HPLC chromatograms of **CC-7** and **CC-8** under 405-nm laser irradiation (0-60 min). (b) The accumulated concentration of chlorambucil drugs released from **CC-7** and **CC-8** upon laser irradiation. (c) The 405-nm visible-light-triggered photolytic and drug release process.

1.3 In vitro cytotoxicity evaluation toward human breast and leukemia cancer cells

The nitrogen mustard, chlorambucil, is a common DNA alkylating agent used for chemotherapy, which could induce nonspecific cell apoptosis via the accumulation of persistent DNA damage. As shown in Figure 4, two human cancer cell lines were selected as the in vitro platform for testing the bioactivity of the CC-conjugates by a colorimetric MTT assay. Figure 4a shows that **CC-7**, a chlorambucil drug conjugate without TPP ligands, possesses concentration-dependent cytotoxicity to the breast cancer BT-474 cells and leukemia Jurkat-T cells in a dark condition, which is very similar to the cytotoxic profile of pristine chlorambucil toward two cell lines (Figure 4b). The half maximum inhibitory concentration (IC_{50}) of **CC-7** was much higher than 80 μM for Jurkat-T cells and approximately 66 μM for BT-474 cells. The result suggests that the **CC-7** is capable of causing cell death under higher dosages, but certain drug resistance to the nitrogen mustard derivatives was found in the two cell lines, particularly the leukemia cells.

Figure 4c shows the cytotoxicity profiles of **CC-8**, a drug conjugate with a TPP ligand that can assist the drug accumulation inside two cell lines. The proliferation of both cells treated with **CC-8** was also effectively suppressed as the dosage increased. Notably, for Jurkat-T cells, the IC_{50} value dramatically decreased to approximately 20 μM, suggesting that the TPP ligand plays a critical role in increasing the bioavailability of **CC**-drug conjugates toward leukemia cells. Moreover, this result also implied that the resistance of the mustard drug was improved by introducing a mitochondria-targeting ligand. It is assumed that the **CC-8** was substantially accumulated in the mitochondria, and the mtDNA lacking of self-repair mechanism could be permanently damaged by the drug conjugates, eventually leading to the cell death.

To further elucidate the cytotoxicity under laser irradiation, two types of cells were treated with chlorambucil, **CC-7**, and **CC-8** for 30 min under lower dosage of 10 μM, at which all the cell viability is higher than 70%. After rinsed with buffer to remove extracellular drug molecules, the cell suspension was exposed to 405-nm LD for 20 min and then cultured in a dark condition for another 48 h. Based on the HPLC analysis, the setup irradiation time allows maximum phototriggered release of the anticancer drugs. As shown in Figure 4d, the control experiment shows that approximately 90% of BT-474 and Jurkat-T cells without drug treatment were survived under laser exposure, indicating the incident light with 405-nm wavelength is harmless for both cell lines. After treating both cell lines with chlorambucil, we found that more than 80% of the cells were still survived upon laser exposure, because the mustard drug is insensitive to 405-nm light; however, after treated with the **CC**-drug conjugates, the breast cancer cells and leukemia cells show different cytotoxic response upon laser irradiation; the BT-474 cells were still insensitive to the incident light, but cell proliferation for the photo-treated Jurkat-T cells was greatly suppressed. The percentage of the viable cells was decreased to approximately 50% and 40% after treated with **CC-7** and **CC-8**, respectively, implying that the IC_{50}

value was lower than 10 μM. In comparison with the cells in the absence of photo-treatment (Figure 4a and 4c), the **CC** moiety serving as a photoresponsive carrier system evidently enhanced the drug potency under the assistance of visible-light illumination, and the drug-conjugates with a TPP ligand shows the optimized antiproliferative activity toward leukemia cell line.[13]

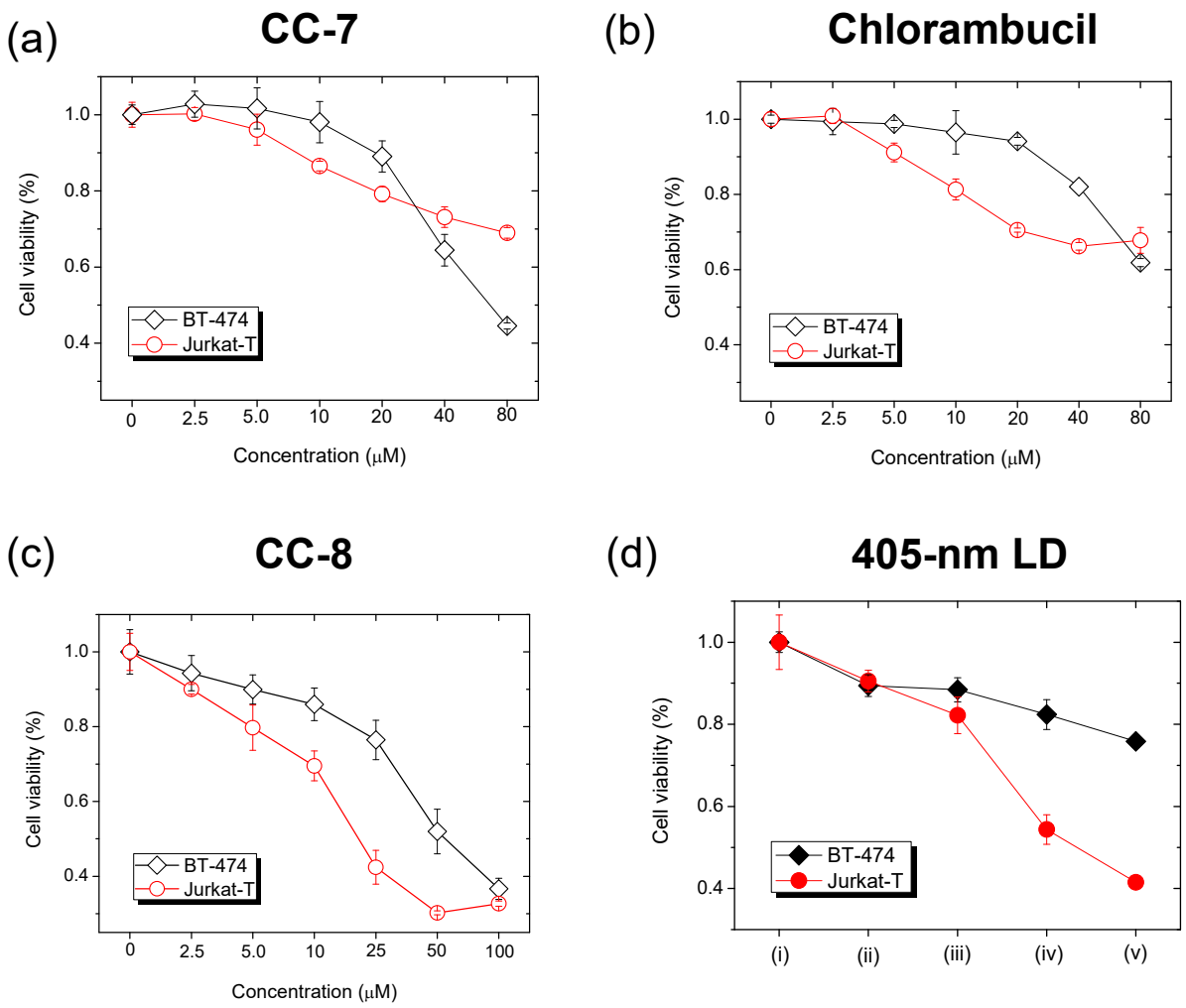

Figure 4. The cytotoxicity in dark condition: (a) **CC-7**, (b) chlorambucil, and (c) **CC-8** toward breast cancer BT-474 (◇) and leukemia Jurkat-T (○) cells; (d) The photo-cytotoxicity under 405-nm laser diode (LD) irradiation: (i) control, (ii) LD only, (iii) chlorambucil + LD, (iv) **CC-7** + LD, (v) **CC-8** + LD toward cancer BT-474 (◆) and leukemia Jurkat-T (●) cells. The drug dosage was 10 μM.

Because the coumarin-based photocages have been proven to possess efficient triplet-triplet absorption at UV-to-visible light region analyzed by the transient spectroscopy, we assumed that the photo-induced antiproliferative activity combines the mustard drug potency and photosensitization effect of the **CC** fused heterocycle.[14] The **CC** moiety may behave like the coumarin photocage, and therefore, quenching the triplet excited state by ground state molecular oxygen ($^3O_2$) to yield cytotoxic singlet oxygen ($^1O_2$) is a possible mechanism to induce cell death. We also assumed that the enhanced potency of **CC**-drug conjugates toward leukemia cells is a synergic effect combining phototriggered anticancer drug release and photosensitization. The simultaneously released chlorambucil and $^1O_2$ contribute equally to the nuclear DNA damage and eventually leads to apoptotic cell death. Moreover, to assess the $^1O_2$, a fluoresceinyl Cypridina luciferin analog (FCLA) was employed as a "turn-on" chemiluminescence probe.[15] The FCLA was readily oxidized by $^1O_2$ and thus markedly enhanced fluorescence by 524 nm. Figure 5a shows that fluorescence of a methanol solution of **CC-7** doped with FCLA probes was gradually increased upon laser irradiation. The emission intensity of FCLA exhibits approximately 1.6-fold increment and plateaued upon irradiation for 10 min. The result is consistent with the UV-vis, fluorescence, and HPLC analysis for the photo-excited **CC**-drug conjugates (Figure 2), confirming that the photocleavage and maximum $^1O_2$ production take place at the same time-scale.

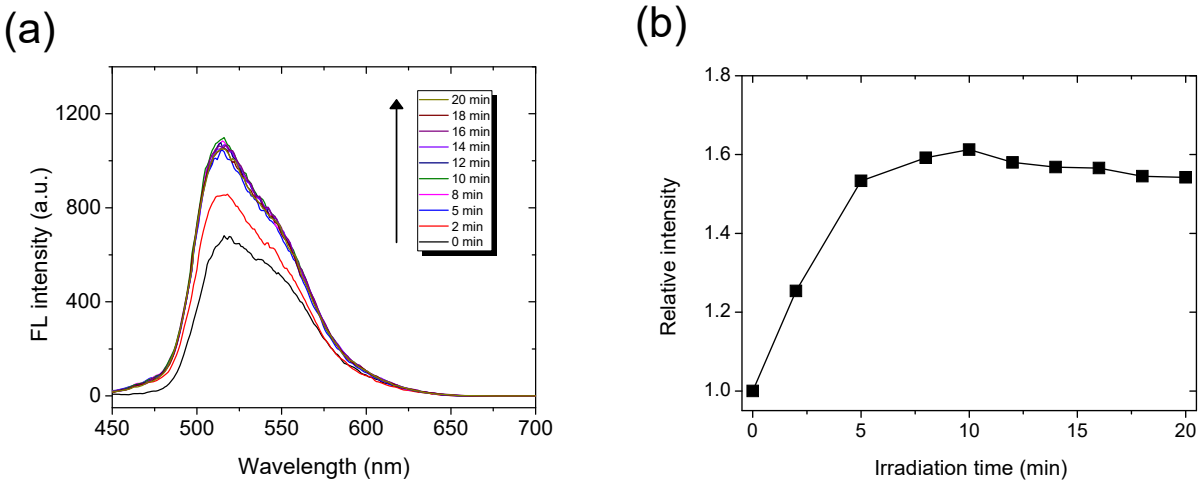

Figure 5. (a) The fluorescence spectra of the FCLA by adding **CC-7** as the photosensitizer upon 405-nm light irradiation (0-20 min). (b) Time courses for the increment of fluorescence intensity under light exposure.

1.4 The mitochondrial stress test in cancer cells treated with CC-drug conjugates

To confirm the mitochondria targeting for **CC-8** with a TPP ligand, we introduced a Seahorse extracellular flux analyzer to monitor the mitochondrial stress through the change in oxygen

consumption and pH value in extracellular microenvironments. Notably, cancer cells are characterized with aerobic glycolysis, which is known as Warburg effect, to generate higher ATP and reactive oxygen species than normal cells by Kerbs cycle.[16] This characteristic also indicates the possible mitochondria dysfunction resulted from the occurrence of mitochondria DNA mutations, and therefore, suppression of mitochrondrial DNA replication also resulted the delayed tumor growth.[17] The acumination of defective mitochondrial respiration was observed in benign tumors but the increased mitochondrial respiration was found to sustain proliferation of malignant tumors.[18] Some reports also suggest that targeting mitochondrial respiration or mitochondrial DNA replication through DNA-alkylating agents (e.g., chlorambucil) may serve as the potential strategies for cancer therapy.[19] As shown in Figure 6a, the real-time trace for oxygen consumption (OCR) in A549 lung cancer cells treated with **CC-8** for 24 h clearly demonstrated decreased basal and maximal respiration (i, iii) and ATP production (ii). When compared to non-treated cells, the OCR values decreased from 142.6±7.2 to 121.2±0.8 and from 98.6±9.8 to 79.3±2.8 pmol/min during basal respiration and ATP production, respectively (Figure 6b). These data implied that **CC-8** could target mitochondria and induce basal level of mitochondrial damage without light exposure. Promisingly, the examination of the mitochondrial DNA replication and cell proliferation after light exposure in the future could further demonstrate full potential of the **CC**-drug conjugates toward cancer therapy.

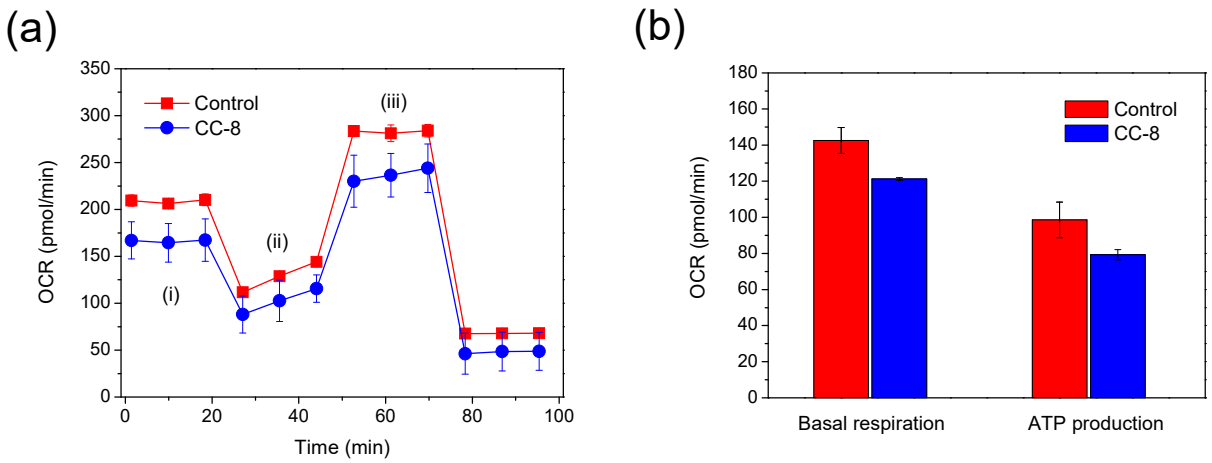

Figure 6. Mitochondrial stress assay determined by a Seahorse extracellular flux analyzer. (a) The real-time trace for oxygen consumption rate (OCR) during (i) basal respiration, (ii) ATP production, and (iii) maximal respiration. Oligomycin and carbonyl cyanide-p-trifluoromethoxyphenylhydrazone (FCCP) were injected at 18- and 44-min for phase transition, respectively. (b) Quantitative analysis for OCR values at basal respiration and ATP production in non-treated and **CC-8**-treared A549 cancer cells.

2. Conclusion

In this paper, we focused on the synthesis of photoresponsive drug carrier based on a carbazole-coumarin heterocycle. This platform permits visible-light-triggered drug release and potentially possesses two-photon absorption behavior. Through a tailor-made synthetic protocol, the chemotherapy drug (chlorambucil) and site–specific targeting ligand (TPP) can be readily conjugated with the coumarin and carbazole moieties, respectively. Compared with the pristine drug, the hybrid drug system considerably improved IC_{50} values toward leukemia Jurkat-T cells under 405-nm laser irradiation. This is presumably due to a synergic effect of phototriggered anticancer drug release and photosensitization of carbazole-coumarin moiety. The study along a mechanistic investigation on mitochondrial targeting and further increasing the drug performance is now in progress.

3. Experimental Section

4.1 Materials and Instruments

The chemical reagents and organic solvents for materials synthesis were obtained as high-purity reagent-grade from commercial suppliers including Sigma-Aldrich and TCI chemicals and used without further purification. ^{1}H (400 MHz) and ^{13}C (75 MHz) NMR spectra were recorded on a Varian Mercury Plus 400 MHz spectrometer at room temperature using $CDCl_3$, DMSO-d_6, methanol-d_4, or D_2O as the solvents. Spectral processing (Fourier transform, peak assignment, and integration) was performed using MestReNova 6.2.1 software. Matrix-assisted laser desorption ionization/time-of-flight (MALDI–TOF) MS was performed on a Bruker AutoFlex III TOF/TOF system in positive ion mode using either 2,5-dihydroxybenzoic acid or α-cyano-4-hydroxycinnamic acid as the desorption matrix. UV-Vis absorption spectra was performed on a Thermo Genesys 10S UV–Vis spectrometer. Fluorescence emission spectra was recorded on a Hitachi F-2500 spectrometer. HPLC was performed on a JASCO instrument equipped with a UV–970 UV–Vis detector covering the wavelengths from 200-900 nm. The HPLC analysis was conducted at 25 ºC using Dr. Maisch ReproSil-100 C18 column (250 x 4.6 mm, reverse phase with 5 um porous spherical silica). A solvent mixture of methanol (90%) and water (10%) was used as a mobile phase and the flow rate was maintained at 1.0 cm^3/min. Photolysis of **CC**-conjugates were carried out by using 405-nm laser diodes under a power density of 1.9 W/cm^2.

4.2 Synthetic Procedures for CC-3

The **CC-3** was synthesized following a modified procedure based on Zheng's report.[8] An ethanol solution of 4-hydroxycarbazole (366.4 mg, 2.0 mmol) and $ZnCl_2$ (381.7 mg, 2.8 mmol) was added by ethyl acetoacetate (840 μL, 6.7 mmol), and the mixture was stirred at 110 ºC under N_2 for 24 h. The mixture was then poured into ice water, and the precipitate was collected and purified by flash column chromatography using solvent gradient elution (ethyl acetate:hexane = 6:4 to 2:8, R_f = 0.3)

to obtain **CC-1** as white solid (20%).^{1}H NMR (400 MHz, DMSO) δ = 11.91 (s, 1H), 8.31 (d, *J* = 7.8 Hz, 1H), 7.74 (d, *J* = 8.6 Hz, 1H), 7.60 (d, *J* = 8.1 Hz, 1H), 7.47 – 7.51 (m, 2H), 7.32 (t, *J* = 7.5 Hz, 1H), 6.28 (s, 1H). ^{13}C-NMR (100 MHz, DMSO): δ = 160.84, 155.57, 150.43, 143.11, 140.19, 126.74, 123.17, 122.85, 121.13, 120.80, 112.23, 111.63, 110.50, 110.01, 108.78, 19.59.

A DMF solution of **CC-1** (327.0 mg, 1.3 mmol), K_2CO_3 (1.267 g, 9.1 mmol) was added dropwise by methyl iodide (1.63 mL, 20 mmol). The mixture was stirred at 50 ºC under N_2 for 24 h. The solvent and volatile were removed by vacuum, and the residue was extracted with CH_2Cl_2 and water. The organic layer was collected and evaporated to dryness to obtain **CC-2** quantitatively. An anhydrous toluene solution of SeO_2 (55.5 mg, 0.5 mmol) and **CC-2** (65.3 mg, 0.25 mmol) was stirred at 110 ºC under N_2 for 48 h. After the reaction was cooled to room temperature, the precipitate was filtered off, and the filtrate was evaporated to dryness. The residue redissolved in anhydrous methanol/THF solutions (20:1) was added dropwise into a methanol solution of $NaBH_4$ (47.3 mg, 1.25 mmol), and stirred at 25 ºC overnight. After neutralized with 1M HCl, the mixture was extracted with ethyl acetate and brine. The organic layer was collected and evaporated to dryness, and the crude was purified by flash column chromatography using solvent gradient elution (CH_2Cl_2:CH_3OH = 99:1 to 97:3, R_f = 0.1) to obtain **CC-3** as white solid (20%).^{1}H NMR (400 MHz, DMSO) δ = 8.33 (d, *J* = 6.9 Hz, 1H), 7.70 – 7.75 (m, 2H), 7.64 – 7.53 (m, 2H), 7.42 – 7.34 (m, 1H), 6.40 (s, 1H), 5.69 (bs, 1H), 4.87 (d, *J* = 5.6 Hz, 2H), 3.95 (s, 3H). ^{13}C-NMR (100 MHz, DMSO): δ = 161.21, 158.72, 150.19, 143.46, 141.02, 126.83, 122.86, 121.98, 121.07, 120.66, 110.57, 109.43, 109.29, 107.04, 106.76, 60.18, 30.15.

4.3 Synthetic Procedures for CC-7

4-hydroxycarbazole (200 mg, 1.09 mmol), ethyl 4-chloroacetoacetate (0.33 ml, 2.45 mmol), and methanesulfonic acid (2.5 ml. 38.1 mmol) were mixed and vigorously stirred for 2 h. The mixture was then poured into ice water to remove excess acid. The precipitate was collected and purified by flash column chromatography (CH_2Cl_2, R_f = 0.4) to obtain **CC-4** as dark-yellow solid (54%). ^{1}H NMR (400 MHz, DMSO) δ = 11.99 (s, 1H), 8.30 (d, *J* = 7.7 Hz, 1H), 7.82 (d, *J* = 8.6 Hz, 1H), 7.61 (d, *J* = 8.1 Hz, 1H), 7.51 (m, 2H), 7.33 (t, *J* = 7.7 Hz, 1H), 6.57 (s, 1H), 5.10 (s, 2H). ^{13}C-NMR (100 MHz, DMSO): δ = 160.11, 152.22, 150.25, 142.53, 139.52, 126.25, 122.30, 122.21, 120.35, 111.69, 110.59, 109.52, 108.39, 54.96, 41.99, 40.15, 39.94, 39.73, 39.52, 39.31, 39.10, 38.89.

A DMF solution of **CC-4** (100 mg, 0.35 mmol), K_2CO_3 (342 mg, 2.47 mmol) was added dropwise by *tert*-butyl bromoacetate (2.6 ml, 17.7 mmol). The mixture was stirred at 60 ºC under N_2 for 24 h. The solvent and volatile were removed by vacuum, and the residue was extracted with CH_2Cl_2 and water. The organic layer was collected and evaporated to dryness. The crude was purified by flash column chromatography (ethyl acetate:hexane = 1:4, R_f = 0.2) to obtain **CC-5** as yellow solid (70%). ^{1}H NMR (400 MHz, $CDCl_3$) δ = 8.55 (d, *J* = 7.9 Hz, 1H), 7.70 (d, *J* = 8.7 Hz, 1H), 7.48 (t, *J* = 7.7 Hz, 1H), 7.37 – 7.27 (m, 2H), 7.24 (d, *J* = 8.7 Hz, 1H), 6.39 (s, 1H), 4.90 (s, 2H), 1.36 (s, 9H). ^{13}C-NMR (100 MHz, $CDCl_3$): δ = 166.71, 160.81, 151.11, 150.77, 143.09, 140.22, 126.60, 123.86,

121.68, 121.32, 121.04, 111.89, 110.98, 109.36, 108.59, 105.61, 83.18, 45.65, 27.93, 27.55.

A DMF solution of chlorambucil (84.1 mg, 0.276 mmol) and K_2CO_3 (41.7 mg, 0.3 mmol) was mixed at room temperature for 30 min. The **CC-5** (100 mg, 0.25 mmol) dissolved in DMF was added dropwise into the mixture, followed by stirring for another 30 min. The solvent and volatile were removed by vacuum, and the residue was purified by flash column chromatography (CH_2Cl_2:CH_3OH = 99:1, R_f = 0.6) to obtain **CC-6** as yellow solid (72%). ^{1}H NMR (400 MHz, $CDCl_3$) δ = 8.56 (d, *J* = 7.9 Hz, 1H), 7.54 – 7.43 (m, 2H), 7.38 – 7.27 (m, 2H), 7.20 (d, *J* = 8.7 Hz, 3H), 7.01 (d, *J* = 8.6 Hz, 2H), 6.56 (d, *J* = 8.6 Hz, 2H), 6.37 (s, 1H), 5.32 (s, 2H), 4.89 (s, 2H), 3.70 – 3.45 (m, 8H), 2.54 (t, *J* = 7.5 Hz, 2H), 2.43 (t, *J* = 7.5 Hz, 2H), 2.07 – 1.84 (m, 2H), 1.35 (s, 9H). ^{13}C-NMR (100 MHz, $CDCl_3$): δ = 172.69, 166.68, 160.95, 150.32, 144.30, 142.84, 140.12, 129.98, 129.66, 126.55, 123.80, 121.21, 120.96, 120.42, 112.02, 110.79, 109.04, 108.53, 105.60, 83.08, 61.28, 53.47, 45.56, 40.46, 33.84, 33.28, 29.64, 27.89, 26.51.

The **CC-6** (120 mg, 0.198 mmol) was mixed with 5 ml of trifluoroacetic acid and stirred for overnight. The volatile was removed by vacuum, and the crude was recrystallized in CH_3OH to obtain **CC-7** as yellow solid (80%). ^{1}H NMR (400 MHz, DMSO) δ = 8.34 (d, *J* = 7.8 Hz, 1H), 7.76 (d, *J* = 8.8 Hz, 1H), 7.69 (d, *J* = 8.2 Hz, 1H), 7.64 (d, *J* = 8.8 Hz, 1H), 7.55 (t, *J* = 7.7 Hz, 1H), 7.39 (t, *J* = 7.5 Hz, 1H), 7.03 (d, *J* = 8.3 Hz, 2H), 6.65 (d, *J* = 8.3 Hz, 2H), 6.35 (s, 1H), 5.48 (s, 2H), 5.37 (s, 2H), 3.68 (s, 8H), 1.97 – 1.69 (m, 2H). ^{13}C NMR (100 MHz, DMSO) δ = 173.04, 170.50, 160.60, 152.41, 150.33, 145.14, 143.76, 141.01, 130.02, 127.05, 122.93, 122.51, 121.54, 120.81, 112.51, 110.77, 109.89, 109.33, 108.49, 107.57, 62.17, 52.84, 45.02, 41.79, 33.93, 33.42, 27.22. MALDI-TOF-MS: Cacld. For $(M+H)^+$ $C_{32}H_{31}Cl_2N_2O_6$: 609.16 Da; Found: 609.33 Da.

4.4 Synthetic Procedure for CC-8

(3-aminopropyl)triphenylphosphonium was synthesized following the reported procedure. [9b,20] An anhydrous DMF solution of **CC-7** (79 mg, 0.129 mmol), HATU (49.3 mg, 0.129 mmol), and Hünig's base (0.23 ml, 1.29 mmol) was added by the phosphonium salt (50 mg, 0.155 mmol), and the mixture was stirred for 3 days under N_2. After complete consumption of the **CC-7**, the solvent and volatile was removed by vacuum, and the crude was purified by flash column chromatography (CH_2Cl_2:CH_3OH = 20:1, R_f = 0.5). The final product was recrystallized in CH_3OH to obtain **CC-9** as yellow solid (50%). ^{1}H NMR (400 MHz, $CDCl_3$) δ = 8.43 (d, *J* = 8.1 Hz, 1H), 7.83 – 7.14 (m, 20H), 7.09 (d, *J* = 8.5 Hz, 2H), 6.63 (d, *J* = 8.5 Hz, 2H), 6.29 (s, 1H), 5.21 (s, 2H), 4.86 (s, 2H), 3.70 (t, *J* = 6.2 Hz, 4H), 3.62 (t, *J* = 6.2 Hz, 4H), 3.41 (m, 2H), 3.04 (m, 2H), 2.61 (t, *J* = 7.4 Hz, 2H), 2.48 (t, *J* = 7.4 Hz, 2H), 2.07 – 1.92 (m, 2H), 1.90 – 1.75 (m, 2H). ^{13}C-NMR (100 MHz, $CDCl_3$): δ = 172.89, 168.37, 161.23, 150.76, 150.24, 144.47, 143.35, 140.37, 135.44, 135.41, 133.27, 133.17, 130.74, 130.61, 130.23, 129.87, 126.69, 123.68, 121.15, 121.01, 120.66, 118.05, 117.19, 112.20, 110.55,

109.20, 108.94, 108.13, 106.41, 77.48, 77.16, 76.84, 61.44, 53.66, 45.85, 40.70, 39.37, 34.03, 33.44, 26.72, 22.06, 20.29, 19.75. MALDI-TOF-MS: Cacld. For M^+ $C_{53}H_{51}Cl_2N_3O_5P$: 910.29 Da; Found: 910.02 Da.

4.5 Cell Viability Assay

Cell proliferation after light exposure were determined by a colorimetric MTT cell viability assay reagent (Sigma-Aldrich) using a microplate reader (Molecular Devices, Sunnyvale, CA, USA) according to the manufacturer's recommendations. For the in vitro photoexicitation experiment, BT-474 and Jurkat-T cell lines were firstly suspended as 1×10^5/ml for 2.5 ml and transferred into a 1-cm quartz cuvette and directly exposed to a laser beam with 405-nm wavelength at fixed time intervals under gentle agitation. The exposed cells were then seeded into 96-well-plate at 1×10^4/well and cultured for another 48 h. The absorbance values at 440 nm of non-treatment control were set as 100% of cell proliferation.

4.6 The Singlet Oxygen Assay

In a typical FCLA experiment, 20 μL of a FCLA/ethanol solution (0.7 mg/mL) was added to 2 mL of a sample solution and transferred into a 1-cm quartz cuvette. The solution was irradiated with a 405-nm laser diode, and the emission intensity of the exposed solutions at 519-nm was recorded every 2 min under 496-nm excitation by fluorescence spectroscopy. For the control experiment, FCLA emission was also recorded at the same conditions in the absence of laser irradiation.

4.7 The mitochondrial stress assay

Seahorse XFe extracellular flux analyzer (Ailgent Technologies, Inc.) is a live cell measurement for determination of mitochondria function by measuring oxygen consumption rate (OCR) and extracellular acidification rate (ECAR) with probes for oxygen and proton. Briefly, A549 cells were seeded into assay wells at a density of 1×10^4 cells/well in bicarbonate-free culture medium for overnight. After loading with inhibitors into automatically releasing injectors (Oligomycin inhibits ATP synthase (complex V), FCCP uncouples oxygen consumption from ATP production, and rotenone and antimycin A inhibit complexes I and III, respectively. All the inhibitors were purchased from Ailgent Technologies, Inc., Santa Clara, CA, USA), inserts with activated probes and inhibitors were inserted into cell-seeded wells and sent into Seahorse Analyzer for measurement. The raw data were outputted and analyzed by the excel template provided by the manufacturer of Seahorse Analyzer.

Notes and reference

1. (a) Timko, B. P.; Dvir, T.; Kohane, D. S., Remotely Triggerable Drug Delivery Systems. *Adv. Mater.* **2010,** *22* (44), 4925-4943; (b) Olejniczak, J.; Carling, C.-J.; Almutairi, A., Photocontrolled

release using one-photon absorption of visible or NIR light. *J. Controlled Release* **2015,** *219*, 18-30; (c) Poelma, S. O.; Oh, S. S.; Helmy, S.; Knight, A. S.; Burnett, G. L.; Soh, H. T.; Hawker, C. J.; Read de Alaniz, J., Controlled drug release to cancer cells from modular one-photon visible light-responsive micellar system. *Chem. Commun.* **2016,** *52* (69), 10525-10528.
2. Karimi, M.; Sahandi Zangabad, P.; Baghaee-Ravari, S.; Ghazadeh, M.; Mirshekari, H.; Hamblin, M. R., Smart Nanostructures for Cargo Delivery: Uncaging and Activating by Light. *J. Am. Chem. Soc.* **2017**.
3.(a) Furuta , T.; Wang, S. S. H.; Dantzker, J. L.; Dore, T. M.; Bybee, W. J.; Callaway, E. M.; Denk, W.; Tsien, R. Y., Brominated 7-hydroxycoumarin-4-ylmethyls: Photolabile protecting groups with biologically useful cross-sections for two photon photolysis. *Proc. Natl. Acad. Sci. U. S. A.* **1999,** *96* (4), 1193-1200; (b) Barman, S.; Mukhopadhyay, S. K.; Gangopadhyay, M.; Biswas, S.; Dey, S.; Singh, N. D. P., Coumarin-benzothiazole-chlorambucil (Cou-Benz-Cbl) conjugate: an ESIPT based pH sensitive photoresponsive drug delivery system. *J. Mater. Chem. B* **2015,** *3* (17), 3490-3497.
4. Eckardt, T.; Hagen, V.; Schade, B.; Schmidt, R.; Schweitzer, C.; Bendig, J., Deactivation Behavior and Excited-State Properties of (Coumarin-4-yl)methyl Derivatives. 2. Photocleavage of Selected (Coumarin-4-yl)methyl-Caged Adenosine Cyclic 3‘,5‘-Monophosphates with Fluorescence Enhancement. *J. Org. Chem.* **2002,** *67* (3), 703-710.
5. Lin, Q.; Bao, C.; Fan, G.; Cheng, S.; Liu, H.; Liu, Z.; Zhu, L., 7-Amino coumarin based fluorescent phototriggers coupled with nano/bio-conjugated bonds: Synthesis, labeling and photorelease. *J. Mater. Chem.* **2012,** *22* (14), 6680-6688.
6. (a) Lin, Q.; Huang, Q.; Li, C.; Bao, C.; Liu, Z.; Li, F.; Zhu, L., Anticancer Drug Release from a Mesoporous Silica Based Nanophotocage Regulated by Either a One- or Two-Photon Process. *J. Am. Chem. Soc.* **2010,** *132* (31), 10645-10647; (b) Lin, Q.; Bao, C.; Cheng, S.; Yang, Y.; Ji, W.; Zhu, L., Target-Activated Coumarin Phototriggers Specifically Switch on Fluorescence and Photocleavage upon Bonding to Thiol-Bearing Protein. *J. Am. Chem. Soc.* **2012,** *134* (11), 5052-5055; (c) Lin, Q.; Bao, C.; Yang, Y.; Liang, Q.; Zhang, D.; Cheng, S.; Zhu, L., Highly Discriminating Photorelease of Anticancer Drugs Based on Hypoxia Activatable Phototrigger Conjugated Chitosan Nanoparticles. *Adv. Mater.* **2013,** *25* (14), 1981-1986.
7. Kitamura, N.; Fukagawa, T.; Kohtani, S.; Kitoh, S.-i.; Kunimoto, K.-K.; Nakagaki, R., Synthesis, absorption, and fluorescence properties and crystal structures of 7-aminocoumarin derivatives. *J. Photochem. Photobiol., A* **2007,** *188* (2), 378-386.
8. Zheng, K.; Lin, W.; Tan, L.; Chen, H.; Cui, H., A unique carbazole-coumarin fused two-photon platform: development of a robust two-photon fluorescent probe for imaging carbon monoxide in living tissues. *Chem. Sci.* **2014,** *5* (9), 3439-3448.
9. (a) Peng, Y. B.; Zhao, Z. L.; Liu, T.; Xie, G. J.; Jin, C.; Deng, T. G.; Sun, Y.; Li, X.; Hu, X. X.; Zhang, X. B.; Ye, M.; Tan, W. H., A Multi-Mitochondrial Anticancer Agent that Selectively Kills Cancer Cells and Overcomes Drug Resistance. *ChemMedChem* **2017,** *12* (3), 250-256; (b) Millard, M.; Gallagher, J. D.; Olenyuk, B. Z.; Neamati, N., A Selective Mitochondrial-Targeted Chlorambucil with Remarkable Cytotoxicity in Breast and Pancreatic Cancers. *J. Med. Chem.* **2013,** *56* (22), 9170-9179; (c) Jung, H. S.; Lee, J.-H.; Kim, K.; Koo, S.; Verwilst, P.; Sessler, J. L.; Kang, C.; Kim, J. S., A

Mitochondria-Targeted Cryptocyanine-Based Photothermogenic Photosensitizer. *J. Am. Chem. Soc.* **2017,** *139* (29), 9972-9978.
10. Smith, R. A. J.; Porteous, C. M.; Gane, A. M.; Murphy, M. P., Delivery of bioactive molecules to mitochondria in vivo. *Proc. Natl. Acad. Sci. U. S. A.* **2003,** *100* (9), 5407-5412.
11. Schmidt, R.; Geissler, D.; Hagen, V.; Bendig, J., Kinetics Study of the Photocleavage of (Coumarin-4-yl)methyl Esters. *J. Phys. Chem. A* **2005,** *109* (23), 5000-5004.
12. Brtouwer, A. M., Standards for photoluminescence quantum yield measurements in solution (IUPAC Technical Report). *Pure Appl. Chem.* **2011,** *83* (12), 2213-2228.
13. Fonseca, Sonali B.; Pereira, Mark P.; Mourtada, R.; Gronda, M.; Horton, Kristin L.; Hurren, R.; Minden, Mark D.; Schimmer, Aaron D.; Kelley, Shana O., Rerouting Chlorambucil to Mitochondria Combats Drug Deactivation and Resistance in Cancer Cells. *Chem. Biol.* **2011,** *18* (4), 445-453.
14. Gangopadhyay, M.; Mukhopadhyay, S. K.; Karthik, S.; Barman, S.; Pradeep Singh, N. D., Targeted photoresponsive TiO2-coumarin nanoconjugate for efficient combination therapy in MDA-MB-231 breast cancer cells: synergic effect of photodynamic therapy (PDT) and anticancer drug chlorambucil. *MedChemComm* **2015,** *6* (5), 769-777.
15. Wang, B.-Y.; Liao, M.-L.; Hong, G.-C.; Chang, W.-W.; Chu, C.-C., Near-Infrared-Triggered Photodynamic Therapy toward Breast Cancer Cells Using Dendrimer-Functionalized Upconversion Nanoparticles. *Nanomaterials* **2017,** *7* (9), 269.
16. Shulman, R. G.; Rothman, D. L., The Glycogen Shunt Maintains Glycolytic Homeostasis and the Warburg Effect in Cancer. *Trends in Cancer* **2017,** *3* (11), 761-767.
17. (a) Battogtokh, G.; Cho, Y.-Y.; Lee, J. Y.; Lee, H. S.; Kang, H. C., Mitochondrial-Targeting Anticancer Agent Conjugates and Nanocarrier Systems for Cancer Treatment. *Frontiers in pharmacology* **2018,** *9*, 922-922. (b) Tan, An S.; Baty, James W.; Dong, L.-F.; Bezawork-Geleta, A.; Endaya, B.; Goodwin, J.; Bajzikova, M.; Kovarova, J.; Peterka, M.; Yan, B.; Pesdar, Elham A.; Sobol, M.; Filimonenko, A.; Stuart, S.; Vondrusova, M.; Kluckova, K.; Sachaphibulkij, K.; Rohlena, J.; Hozak, P.; Truksa, J.; Eccles, D.; Haupt, L. M.; Griffiths, L. R.; Neuzil, J.; Berridge, Michael V., Mitochondrial Genome Acquisition Restores Respiratory Function and Tumorigenic Potential of Cancer Cells without Mitochondrial DNA. *Cell Metabolism* **2015,** *21* (1), 81-94.
18. Zong, W.-X.; Rabinowitz, J. D.; White, E., Mitochondria and Cancer. *Mol. Cell* **2016,** *61* (5), 667-676.
19. (a) Wilson, G. L.; LeDoux, S. P.; Beecham, E. J.; Wassermann, K.; Stevnsner, T.; Bohr, V. A., Repair of mitochondrial DNA after various types of DNA damage in Chinese hamster ovary cells. *Carcinogenesis* **1992,** *13* (11), 1967-1973; (b) Cullinane, C.; Bohr, V. A., DNA Interstrand Cross-Links Induced by Psoralen Are Not Repaired in Mammalian Mitochondria. *Cancer Res.* **1998,** *58* (7), 1400.
20. Zhou, P.; Yao, J.; Hu, G.; Fang, J., Naphthalimide Scaffold Provides Versatile Platform for Selective Thiol Sensing and Protein Labeling. *ACS Chem. Biol.* **2016,** *11* (4), 1098-1105.

附錄二

Full Paper

Oligopeptide-Side Chained Alginate Nanocarrier for Melittin-Targeted Chemotherapy

Karnthidaporn Wattanakul,[†] Toyoko Imae,*[†‡] Wen-Wei Chang,[§] Chih-Chien Chu,*[#ç] Rina Nakahata[ǁ] and Shin-ichi Yusa[ǁ]

———————

[†]Graduate Institute of Applied Science and Technology, National Taiwan University of Science and Technology, Keelung Road, Taipei 10607, Taiwan
[‡]Department of Chemical Engineering, National Taiwan University of Science and Technology, Keelung Road, Taipei 10607, Taiwan
[§]Department of Biomedical Sciences, Chung Shan Medical University, Jianguo N. Rd., Taichung 40201, Taiwan
[#]Department of Medical Applied Chemistry, Chung Shan Medical University, Jianguo N. Rd., Taichung 40201, Taiwan
[ç]Department of Medical Education, Chung Shan Medical University Hospital, Taichung 40201, Taiwan

[ǁ]Department of Materials Science and Chemistry, University of Hyogo, Himeji, Hyogo 671-2280, Japan

———————

*Corresponding Author: Chih-Chien Chu

Department of Medical Applied Chemistry

Chung Shan Medical University

No. 110, Sec. 1, Jianguo N. Rd., Taichung 40201, Taiwan

TEL/FAX: +886-4-2324-8189; E-mail: **jrchu@csmu.edu.tw**

Abstract

Melittin-target drug carrier was successfully synthesized by chemical binding of sodium alginate with oligopeptide via amidation method at different oligopeptide:alginate unit mole ratio. The average sizes of oligopeptide-alginate nanoparticles in the presence of 1 mM $CaCl_3$ decreased with increasing the origopeptide content, indicating intramolecular interaction between oligopeptide-side chains. While the doxorubicin-loading efficiency on nanoparticles (0.1:1) was like that on alginate nanoparticles, the melittin-loading on oligopeptide-alginate nanoparticles (0.1:1) was more than double higher than that on alginate nanoparticles, suggesting the specific interaction of melittin with oligopeptide-side chain in oligopeptide-alginate nanoparticles. While 2.5 μM free melittin was almost no damage to Caco-2 cells, more than 80% of cells was not survived under the dosage of 2.5 μM melittin-loaded oligopeptide-alginate nanoparticles. Results confirm that the derivation of oligopeptide-side chain in alginate offers the specific binding site for melittin and effectively works on cancer chemotherapy.

Keywords: oligopeptide-side chained alginate, nanocarrier, melittin-targeted chemotherapy, drug delivery system, Caco-2 cell.

1. Introduction

Chemotherapy has been a mainstay of cancer treatment for decades. However, most of conventional chemotherapeutic drugs are toxic to healthy cells, and others are hard penetrating in cytotoxicity-inducing tumors. Therefore, the targeted drug delivery is the offered method for drug administration, which is very promising alternative for increasing the concentration of the drug at the desired sites of target without destroy of other normal tissues.[1,2] This kind of function leads to a special focus of nanomedicine, because nanoparticles have a larger surface area-to-volume ratio resulting in a greater efficiency on drug delivery and a better penetrating ability.[3-5] On cancer treatment, the nanoparticles have been developed to fill the enhanced permeability and retention (EPR) effect for passive targeting ability to tumor tissues and also increase the capability to realize active targeting through incorporation of ligands.[6-8] Accordingly, various polymeric materials can be used to develop nanoparticle carriers, because polymeric nanoparticles can protect drugs from rapid metabolism and selectively accumulate in tumor tissues via the EPR effect.

Alginate has attracted much attention as a delivery carrier for cancer therapy due to its significant biological properties, such as biocompatibility, low immunogenicity, non-toxicity, and water-solubility. Furthermore, alginate is a linear anion polysaccharide composed of alternating blocks of 1,4-linked hexuronic acid residues, namely β-D-mannuronate (M) and α-L-glucuronate (G) residues, which possess specific structure and show a pH-dependent swelling behaviour. The carboxyl group transforms from the protonated state to the deprotonated states around pH ~ 5, which allows the neutral polymer to shrink in the acidic pH and the charged polymer to swell in the neutral or basic pH. However, its low encapsulation efficiency and fast release of drug have been observed with alginate microcapsules.[9,10]

Melittin, a major peptide constituent of bee venom, is one of the potential anticancer candidate, because cancer cells are less likely to develop resistance to a membrane-pore former. Thus, melittin has the ability to induce cell cycle arrest, growth inhibition, apoptosis and necrosis in various cancer cells.[11-13] The chemical formula of melittin is $C_{131}H_{228}N_{38}O_{32}$, which consists of the known 26 amino acid sequence, Gly-Ile-Gyl-Ala-Val-Leu-Lys-Val-Leu-The-The-Gly-Leu-Pro-Ala-Leu-Ile-Ser-Trp-Ile-Lys-Arg-Lys-Arg-Gln-Gln.[14,15]

Therefore, in this study, oligopeptide-side chained alginate nanoparticles were synthesized from water soluble alginate and oligopeptide of α-alanine to obtain melittin-targeted drug delivery. The physicochemical characteristics of oligopeptide-side chained alginate nanoparticles were determined using nuclear magnetic resonance (NMR), Fourier transform infrared (FTIR) absorption spectroscopy, and static and dynamic light scattering (SLS and DLS). The characteristics as a drug carrier was compared between melittin and doxorubicin (DOX). The specific effectivity of oligopeptide-side chain on melittin-delivery was discussed in association with cell viability.

2. Materials and methods

2.1 Reagents

Sodium alginate (SA, 216.12 g/unit mol), n-hydroxysuccinimide (NHS), and 1-3-

dimethylaminopropyl-3-ethylcarbodiimide (EDC) were purchased from Acros, (Belgium), and *tert*-butoxycarbonyl (BOC)-alanine monopeptide was obtained from Protein Research Foundation (Japan). Melittin and DOX hydrochloride were supplied from Sigma-Aldrich (USA). All other chemical reagents obtained from commercial sources and used in the study were analytical grade.

2.2 Synthesis of alginate with oligopeptide-side chain (oligopeptide-alginate)

Synthesis of oligopeptide-alginate was performed through four steps as illustrated in Scheme 1. In the first step, to 1 mmol of BOC-alanine (compound (1)) dissolved in dimethylformamide (DMF), equimolar NHS and EDC were added under continuous stirring, and then equimolar propylamine was added into the mixture. After the mixture was stirred at room temperature for 24 h, the solution was added into the mixture of diethy ether and hexane (1:1 by volume) to precipitate the compound (2). The collected compound (2) was supplied for the second step.

The BOC terminal of compound (2) was deprotected by using 5 M HCl in isopropanol: The solution was stirred at 50 ºC for 4 h and the pH of solution was adjusted to pH 7-8 by using a saturated $NaHCO_3$ solution at the end of the reaction. After the solution was cooled down to 20 ºC, the organic solvent phase was collected and then added to the mixture of diethyl ether and hexane (1:1 by volume) to precipitate and obtain the required compound (3).

To prepare the Ala-Ala dipeptide, BOC-alanine was reacted with compound (3) by using amidation method in DMF: One mmol of NHS and equimolar of EDC were added into the BOC-alanine solution and then compound (3) was added. The solution was continuously stirred at room temperature for 24 h. Then, the solution was poured into the mixture of diethyl ether and hexane (1:1 by volume) to obtain the compound (4).

In the last step to obtain the required compound (5), BOC terminal of compound (4) was deprotected by means of the same procedure as the production of compound (3).The yield of each step is described in Scheme 1. The yield was always enough high.

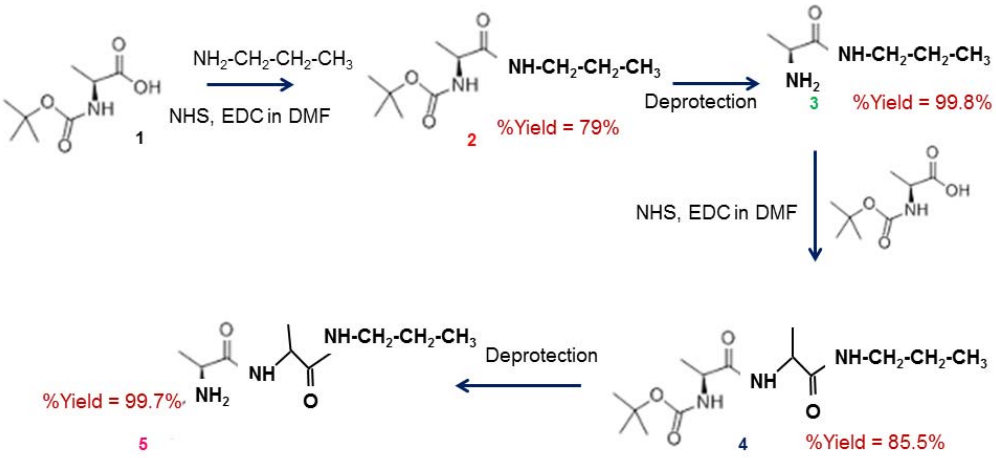

Scheme 1. Synthesis processes of oligopeptide.

The obtained oligopeptide was further used to prepare the oligopeptide-alginate by amidation method in DMF as shown in Scheme 2. At first, 1 mmol of NHS and equimolar of EDC were added

into the alginate solution and then compound (5) was added with various mole ratios (0.033:1, 0.05:1 and 0.1:1 mole ratio of oligopeptide molecule:alginate repeating unit). The solution was continuously stirred at room temperature for 24 h. Then, the solution was poured into the mixture of diethyl ether and hexane (1:1 by volume) to obtain the oligopeptide-alginate.

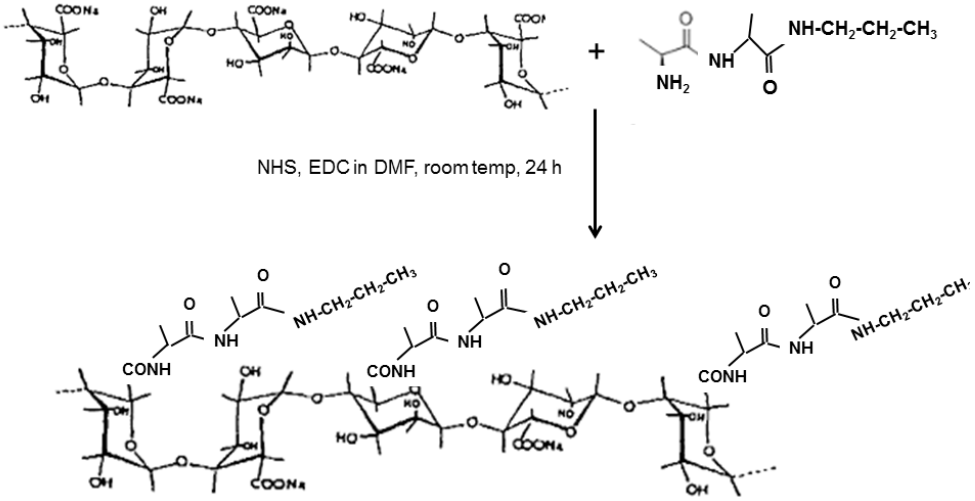

Scheme 2. Synthesis process of oligopeptide-alginate.

2.3 Preparation of alginate and oligopeptide-alginate nanoparticles

To obtain calcium ion-induced alginate nanoparticles, sodium alginate solutions at different concentrations (0.01, 0.075, and 0.1 mg/ml) were prepared by dissolving proper amounts of sodium alginate powder in water at 30 ºC. Then 50 µl of 0.02 M $CaCl_2$ were dropwise added to the stirred aqueous solution (1 ml) of sodium alginate, and the mixture was continuously stirred for 2 h at 30 ºC. Then the concentration of $CaCl_2$ in the prepared solution is 1 mM. Correspondingly, an oligopeptide-alginate solution at a concentration of 0.1 mg/ml was prepared by dissolving oligopeptide-alginate powder in water at 30 ºC. Then 50 µl of 0.02 M $CaCl_2$ was dropwise added to the stirred aqueous solution (1 ml) of oligopeptide-alginate and then continuously stirred for 2 h at 30 ºC.

2.4 Characterization

The ^{1}H-NMR measurement was performed at room temperature on an AVANCE III HD600 nuclear magnetic resonance spectrometer (Bruker) using a 5 mm NMR tube. The alginate and oligo-alginate were dissolved in D_2O (99.9%) to a concentration of 10 mg/ml. The FT-IR absorption spectra on KBr disks were recorded using a Thermo scientific Nicolet 6700 FTIR spectrophotometer at 64 scans (resolution = 4 cm^{-1}).

The static light scattering (SLS) measurement was performed at 25 ºC on an Otsuka Electronics Photal DLS-7000 (Japan) equipped with a He-Ne laser (10 mW at 633 nm) as a light source. The weight-average molecular weight (M_w) and *z*-average radius of gyration (R_g) were evaluated from the Debye plot. The refractive index increment against the concentration (dn/dC_p) at 633 nm was

measured at 25 ºC on an Otsuka Electronics Photal DRM-3000 (Japan). Sample solutions were filtered with a 0.2 μm pore size membrane filter. The zeta potential and DLS were measured using a HoribaMalvern Nano-ZS90 (Japan) with a He-Ne laser beam at 633 nm at 25 ºC. The value was recorded as the average of three measurements.

2.5 Loading and release of drugs on alginate and oligopeptide-alginate nanoparticles

To load drugs in alginate and oligopeptide-alginate nanoparticles, aqueous solutions of DOX (500 μl) or melittin (100μl) at different concentrations of 1-100 μg/ml were incubated with an aqueous solution (1 ml) of alginate or oligopeptide-alginate. All solutions were gently stirred at room temperature for 24 h in the dark. Then, 50 μl of 0.02 M $CaCl_2$ were dropwise added to the stirred aqueous mixture and then continuously stirred for 2 h at 30 ºC under the dark condition.

The drug-loaded nanoparticle solutions were dialyzed in a cellulose tubular membrane (MWCO of 6000-8000 g/mol) against water for 72 h to remove unbound drugs. The amount of unbound drugs in the dialyzed outer solution was determined quantitatively from absorbance of a band (485 nm) of DOX or a band (280 nm) of melittin using a calibration curve. The amount of loaded drug was evaluated by subtracting the amount of unbound drug from the initial amount of drugs.

Controlled release of drugs was examined in a phosphate buffered saline (PBS) at pH 5.5 and 7.4. A nanoparticle solution in a dialysis membrane (MWCO = 3500 g/mol) was dialyzed in 10 ml of water under constant stirring for 72 h at room temperature. The concentration of drugs released into water from the nanoparticle solution was quantified using absorbance at an absorption band of 485 nm for DOX and of 280 nm for melittin.

2.6 Cell viability of alginate and oligopeptide-alginate nanoparticles

Caco-2 cells were obtained from the American Type Culture Collection (ATCC, Manassas, VA) and cultured in DMEM medium (Life Technologies Corporation) supplemented with 10 % fetal bovine serum (Life Technologies Corporation), bovine insulin (5 μg/ml, Sigma-Aldrich), sodium pyruvate (1 mM, Biological Industries), antibiotics (100 unit/ml penicillin and 100 μg/ml streptomycin, Life Technologies Corporation) and Glutamax (2 mM, Life Technologies Corporation). The cells were then grown in 96-well plate at a density of 1×10^4 cells per well. After incubation for 24 h, the sample solutions were added into each well to attain the desired concentrations. After incubation at 37 ºC for 48 h, a solution of 2-(4-iodophenyl)-3-(4-nitrophenyl)-5-(2,4-disulfophenyl)-2H-tetrazolium salt (WST-1) as 10 μl/well was added and the mixture was incubated at 37 ºC for another 3 h. The viability of the cells was determined by visible absorbance at 440 nm after subtracting the reference absorbance at 650 nm with an ELISA microplate reader (EZ Read 400, Biochrom Ltd., Cambridge, UK). Three independent experiments were performed, and each experiment was done in triplicate.

3. Results and discussion

3.1 Characterization of oligopeptide-alginate nanoparticles

Alanine dipeptide was synthesized by using BOC-alanine as a starting material. Figure 1 shows FT-

IR absorption spectra of compound 1-5, the chemical structures of which were illustrated in Scheme 1. An absorption band of BOC-alanine (compound (1)) observed at 3350 cm^{-1} can be assigned to the NH and OH stretching vibration modes and the absorption bands observed at 1717 and 1719 cm^{-1} can be assigned to C=O stretching vibration mode from urethane and carboxylic acid groups. After the reaction of BOC-alanine with trimethylamine, new absorption bands were observed at 1640 and 1520 cm^{-1} assigned to amide I and amide II modes of compound (2), respectively.[16-19] After the deprotection of BOC to obtain compound (3), the absorption bands were observed at 1685 and 1480 cm^{-1}, which were assigned to the C=O stretching and NH_2 bending vibration modes of alanine dipeptide. Similar variation bands of IR absorption spectra occurred even on the process of the syntheses of compounds (4) and (5), where the amidation and the deprotection reactions, respectively, were performed. Thus, similar bands to those of compounds (2) and (3) were obtained at 1614 and 1543 cm^{-1} for compound (4) and 1682 and 1493 cm^{-1} for compound (5).

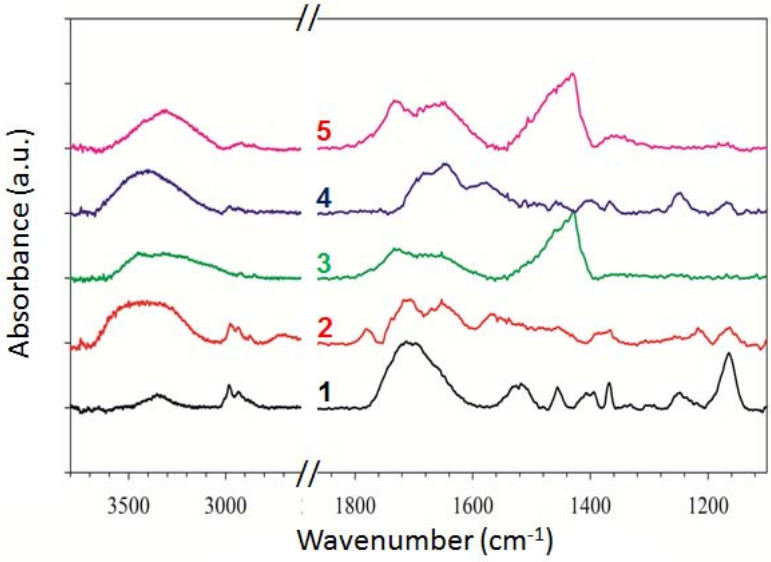

Figure 1. FT-IR absorption spectra of compounds 1-5.

The oligopeptide-alginates with different mole ratios (0.033:1, 0.05:1 and 0.1:1) of oligopeptide to alginate chain unit were prepared. Figure 2 shows the IR absorption spectra of alginate and oligopeptide-alginates. The characteristic IR bands of alginate appeared at 3410, 1644 and 1462 cm^{-1} attributed to the O-H stretching and the carboxylate antisymmetric and symmetric stretching vibration modes, respectively. A small band at 2864 cm^{-1} can be assigned to the C-H stretching vibration mode. While these characteristic bands of alginate can be observed even for oligopeptide-alginates, the shoulder bands at 1694 and 1583 cm^{-1} were observed for oligopeptide-alginates. These bands can be assigned to amide I and II modes, respectively, originated from oligopeptide,[20,21] and these shoulders were clearly observed, when the mole ratio of oligopeptide to alginate is 0.1:1.

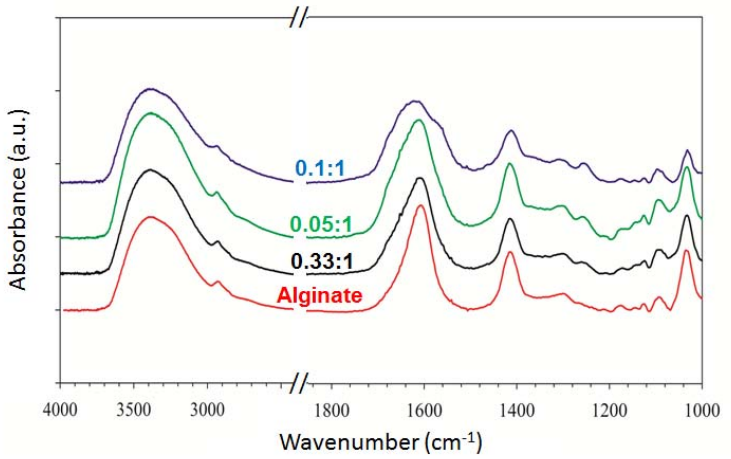

Figure 2. FT-IR absorption spectra of alginate and oligopeptide-alginates.

The successful modification of alginate was also confirmed by ^{1}H-NMR. In Figure 3, the proton chemical shift at 3.63 ppm can be assigned to the proton of alginate. However, the additional proton chemical shifts of oligopeptide-alginate (at 0.1:1) were observed below this chemical shift and were assigned to the methyl, methylene and Cα protons of oligopeptide. Besides, Figure 3 exhibited a signal relative to be presence of the proton of amide group at 4.88 ppm.[22]

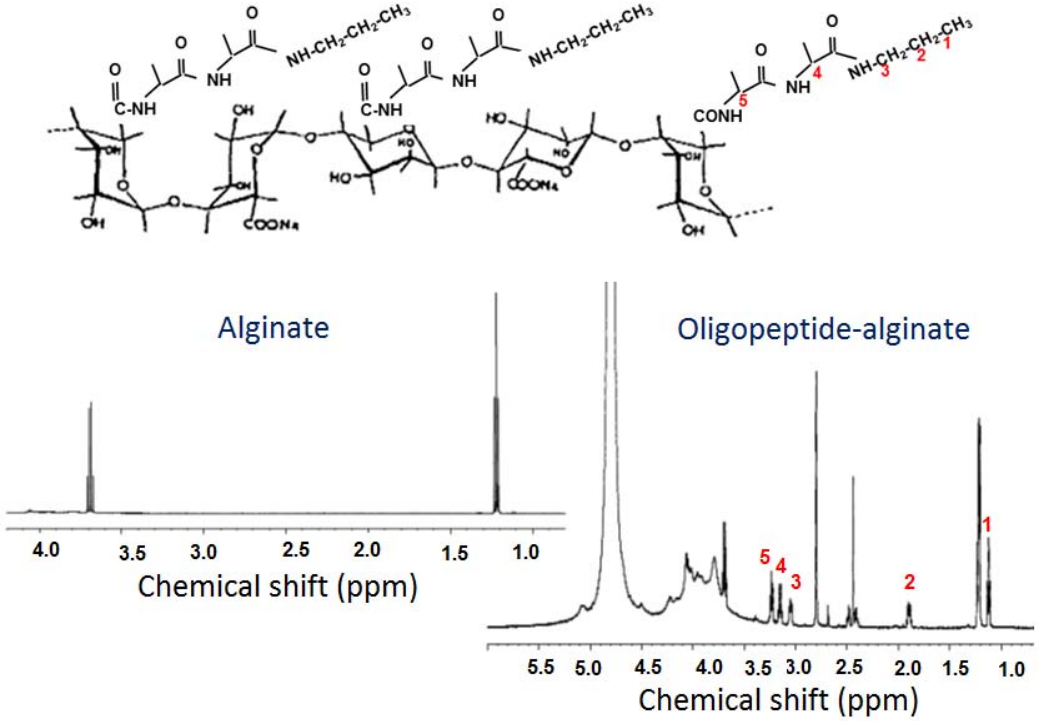

Figure 3. ^{1}H-NMR spectra of alginate and oligopeptide-alginate (0.1:1).

3.2 Sizes of alginate and oligopeptide-alginate nanoparticles

Weight-average molecular weight (M_w), hydrodynamic radius (R_h) and *z*-average radius of gyration (R_g) were evaluated from SLS and DLS measurements performed for alginate and oligopeptide-

alginate (0.1:1) (0.1 mg/ml) in aqueous 0.01 M NaCl solutions at pH 9. The light scattering data, M_w and R_g, from extrapolation of Debye plot to scattering angle (θ) → 0° and the slope of the Debye plot, respectively, are summarized in Table 1 as well as values of R_h and refractive index increment (dn/dC_p, C_p is the polymer concentration). The polymerization degree of alginate estimated from M_w value was 940 and the increase in molecular weight of oligopeptide-alginate is attributed to the substitution of alginate monomer units by oligopeptide. The R_g/R_h values were 1.50 and 1.14, suggesting that the polydispersity of oligopeptide-alginate(0.1:1) was less than that of alginate. The density (d) calculated from M_w and R_h was 0.76 and 0.13 mg/cm^3, respectively, for alginate and oligopeptide-alginate (0.1:1). These small d values indicate that the aggregates contain much water and this character is advantageous for loading small molecule like drugs. The SLS measurement was performed even for oligopeptide-alginate(0.1:1) in an aqueous 1mM $CaCl_2$ solution. The increase of M_w and R_g values (see Table 1) indicates the agglomeration of oligopeptide-alginate(0.1:1). The calculated aggregation number was 37.

Table 1. Weight-average molecular weight (M_w), z-average radius of gyration (R_g), hydrodynamic radius (R_h) and refractive index increment against concentration (dn/dC_p) for alginate and oligopeptide-alginate(0.1:1) (0.1 mg/ml) in an aqueous 0.01 M NaCl solution at pH 9 and for oligopeptide-alginate(0.1:1) (0.1 mg/ml) in an aqueous 1 mM $CaCl_2$ solution.

	$M_w \times 10^5$ (g/mol)	R_g (nm)	R_h (nm)	R_g/R_h	dn/dC_p (ml/g)
Alginate in NaCl	1.65	66.5	44.2	1.50	0.155
oligopeptide-alginate(0.1:1) in NaCl	2.02	96.3	84.2	1.14	0.179
oligopeptide-alginate(0.1:1) in $CaCl_2$	75.6	149			0.103

The hydrodynamic sizes ($2R_h$) in aqueous solutions at the absence and presence of 1 mM $CaCl_2$ were evaluated for alginate and oligopeptide-alginates at different oligopeptide:alginate unit mole ratios. The sizes (685~724 nm in water and 201~248 nm in 1 mM $CaCl_2$) of alginate were almost independent of alginate concentration (0.01~0.1 mg/ml), although the alginate in water was shrunk about 1/3 after adding 1 mM $CaCl_2$. These results are not amazing, if the ionic cross-linkage occurs: The sodium alginate molecules were crosslinking in the existence of Ca ions due to coupling of Ca ions with two carboxylate ions in an alginate molecule.[23] Thus, alginate molecules in $CaCl_2$ solution cannot expand by electrostatic repulsion between free carboxylate, which happened in the solutions in the absence of $CaCl_2$. It can be noted that such size variation of alginate depends on a kind of added salt but does not depend on alginate concentration.

The average sizes of oligopeptide-alginate nanoparticles in an aqueous 1 mM $CaCl_2$ solution evaluated from DLS were 296, 180, 125 and 54 nm at different oligopeptide:alginate unit mole ratios (0:1, 0.033:1, 0.05:1, and 0.1:1), respectively, indicating the decrease of particle size with increasing oligopeptide content. This can be attributed to the less negative charge on the alginate chain after the

reaction of carboxyl group on alginate with the amine group of oligopeptide, leading to be less repulsive within alginate chain.[24] Another possibility is the interaction between oligopeptide-side chains in oligopeptide-alginates. This phenomenon is largely possible, because oligopeptide can form β-sheet by hydrogen bonding.[25,26]

As shown in Figure 4(a), the zeta potential of both alginate and oligopeptide-alginate nanoparticle(0.1:1) in an aqueous 1 mM $CaCl_2$ solution was neutral at acidic media and negative (-34 to -36 mV) at neutral and alkaline (pH 6-11) conditions, because all carboxyl groups in alginate and oligopeptide-alginate are protonated at acidic media and deprotonated to be negatively charged on the particle surface at neutral and alkaline conditions, although the pKa values of carboxyl group were 4.1 and 3.2, respectively, for alginate and oligopeptide-alginate(0.1:1).

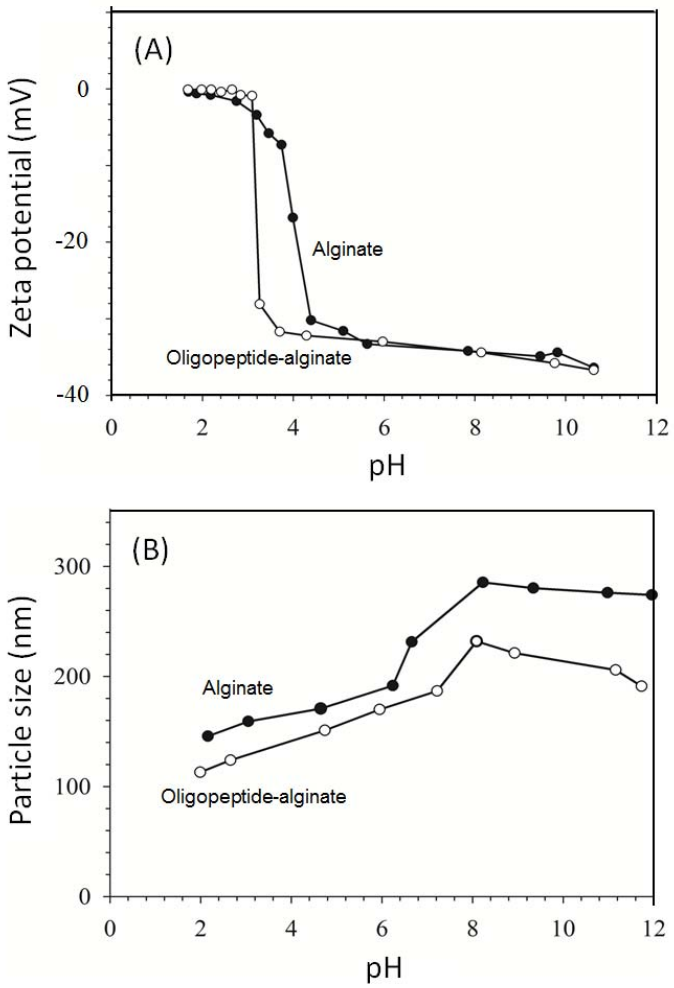

Figure 4. The pH dependence of (a) zeta potential and (b) particle size of alginate and oligopeptide-alginate(0.1:1) nanoparticles.

In addition, it can be known from Figure 4(b) that the changing of pH in aqueous solution also effects on the hydrodynamic particle size of nanoparticles, because alginate nanogel is pH-responsive anionic nanoparticle. At acidic condition below pKa (4.1) of alginate, the majority is COOH group, which results in less electrostatic repulsion on the alginate chain. At elevated pH, the COOH groups are deprotonated to COO^-, which increases the electrostatic repulsion among charges

on the alginate chain, leading to the swelling, namely, the increasing particle size of alginate nanogels.[27,28] Since the carboxyl groups in alginate are partly substituted by oligopeptide-side chain, total amount of carboxyl groups on oligopeptide-alginate are less than pristine alginate and, additionally, there is the attractive interaction between oligopeptide, as described above. Therefore, the particle size of oligopeptide-alginate is always smaller than that of alginate. However, the pH dependence of hydrodynamic size cannot be explained by the aggregate formation, because less charged polymers easy aggregate by less electrostatic repulsion and vice versa. In this situation, the hydrodynamic size must be larger at acidic condition than at alkaline condition, and the results on Figure 4(b) are not coincided with this assumption.

3.3 Drug loading and release on alginate and oligopeptide-alginate nanoparticles

To assess the effectiveness as a drug nanocarrier, the amount of drug loading is one of the barometers. Therefore, the loading efficiency on alginate and oligopeptide-alginate nanoparticles was evaluated by comparing between DOX and melittin. The amount of drug loading on nanoparticles, that is, nanocarriers was plotted as a function of drug concentration as shown in Figure 5. The results demonstrate that the drug loading onto both nanocarriers initially increased by increasing drug concentration, but it's increase was loosened at higher drug concentrations for both drugs. The difference of melittin from DOX is distinct on drug loading amount: While the loading mount of DOX was only 10 % higher on oligopeptide-alginate than on alginate, the melittin loading on oligopeptide-alginate was more than twice higher than on alginate. This variance should be due to the difference on interaction of drugs with nanocarriers: The DOX loading happens mainly by the interaction between carboxylic group on alginate structure and amine group on DOX and, thus, the difference between alginate and oligopeptide-alginate is less. In contrast, the oligopeptide-side chain in alginate induces the hydrogen bonding interaction with peptide groups in melittin structure, but alginate backbone does not arise such specific interaction with melittin.

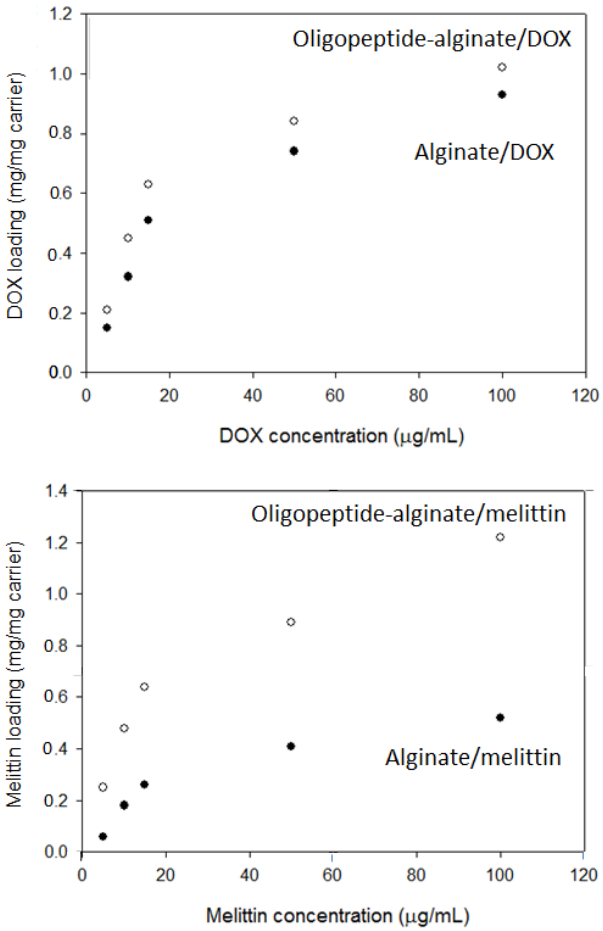

Figure 5. (Top) DOX and (bottom) melittin loading on alginate and oligopeptide-alginate(0.1:1) nanoparticles.

To evaluate the in vitro drug release efficiency of alginate and oligopeptide- alginate nanoparticles, the release of drug from drug-loaded nanoparticles was investigated in PBS solutions at pH 5.5 and 7.4 to be mimic tumor environment and physiological pH in body fluid, respectively.[29] As seen in Figure 6, the drug release increased with the initial time increase up to 10 h and reached to constant values at longer time. The saturated constant release efficiency after 24 h was listed in Table 2 with loading efficiency. It should be noticed that the efficiency by both carriers and drugs were higher at pH 5.5 than at pH 7.4, and especially the difference between efficiency at pH 5.5 and 7.4 for both drugs was larger for oligopeptide-alginate nanoparticles than for alginate nanoparticles. These results indicate the preferable adaptability of oligopeptide-alginate nanoparticles as drug delivery carrier than alginate nanoparticles. However, the melittin release from oligopeptide-alginate nanoparticles was less than that from alginate nanoparticles and the DOX release from oligopeptide-alginate nanoparticles It can be suggested that there is an interaction (maybe, hydrogen bonding) between peptide in melittin and oligopeptide in oligopeptide-alginate, resulting in less melittin release from oligopeptide-alginate nanoparticles.

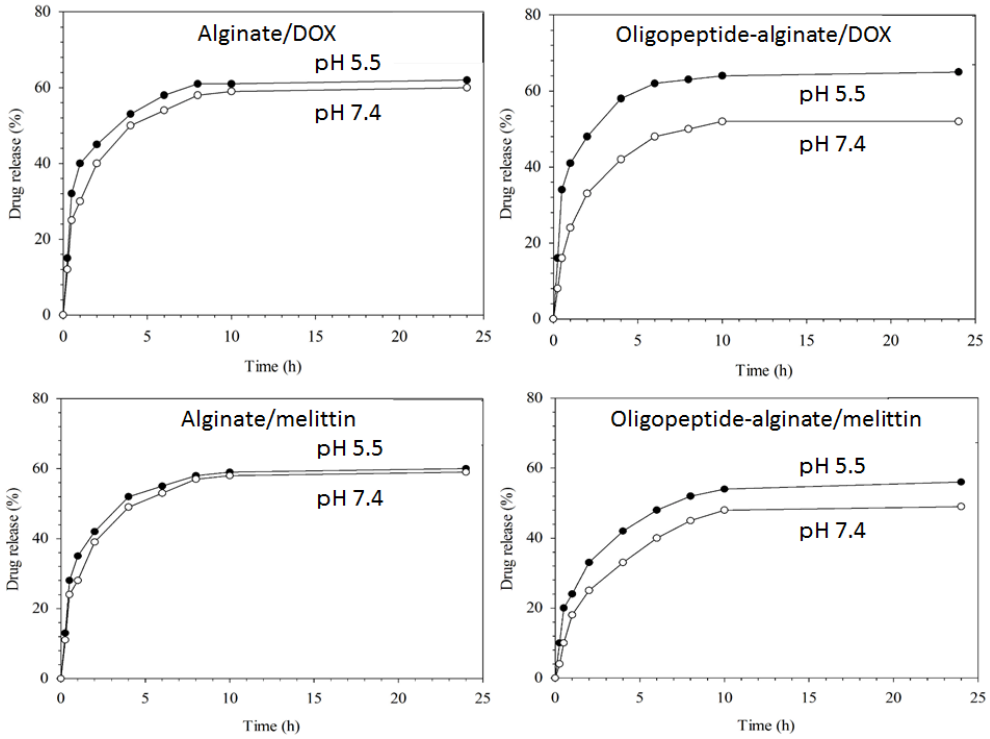

Figure 6. Drug (DOX and melittin) release from alginate and oligopeptide-alginate nanoparticles at pH 5.5 and 7.4.

Table 2 The comparison for drug loading and release between alginate and oligopeptide-alginate nanoparticles. Numerical values indicate efficiency (%). Numerical values in bracket is described by a unit of mg/mg carrier.

Carrier	DOX			Melittin		
	loading	release		loading	release	
		pH5.5	pH7.0		pH5.5	pH7.0
Alginate nanoparticle	93(0.96)	63	60	75(0.52)	59	58
Oligopeptide-alginate nanoparticle	96(1.05)	65	53	98(1.22)	52	46

3.3 Cell viability of drug-loaded alginate and oligopeptide-alginate nanoparticles

The cytotoxicity of free DOX and DOX-loaded oligopeptide-alginate for Caco-2 cell lines is shown in Figure 7(A). The results reveal that approximately 50% of cells was killed under only 0.4 μM of DOX, which is close to the effective IC50 value of this chemotherapy drug for treating the gastrointestinal cells. However, the case using the oligopeptide-alginate as a carrier did not enhance the drug performance. In contrast, the results of the cell viability after treating with free melittin and melittin-loaded oligopeptide-alginate carrier showed significant difference. As seen in Figure 7(B), the oligopeptide-alginate carrier provided almost no damage to the Caco-2 cells, and more than 80% of cells was survived under the dosage of 2.5 μM free melittin. When identical amount of the melittin was loaded onto the oligopeptide-alginate, the hybrid nanoparticle system killed 80% of

Caco-2 cells. As the concentration of melittin was increased to 5 μM, the cells were completely destroyed by both free melittin and melittin-loaded oligopeptide-alginate. The preliminary result suggests that the oligopeptide-alginate could decrease the IC50 value of the melittin for the Caco-2 cells, and potentially makes the melittin on oligopeptide-alginate more effective in clinical cancer therapy.

Although the mechanism regarding how the alginate carrier assists the in vitro performance of the peptide drug is not established, we can speculate that the binding affinity between the melittin and the oligopeptide-alginate is crucial. The driving force of the DOX (chemical drug) loading on the oligopeptide-alginate nanoparticles is mainly physical adsorption, but the melittin (peptide drug) may be adsorbed by the oligopeptide-side chains through more specific interactions (e.g., hydrogen bonding). Therefore, the cellular uptake efficiency and bio-distribution of the melittin could be increased by using the oligopeptide-alginate nanoparticles as the drug carrier.

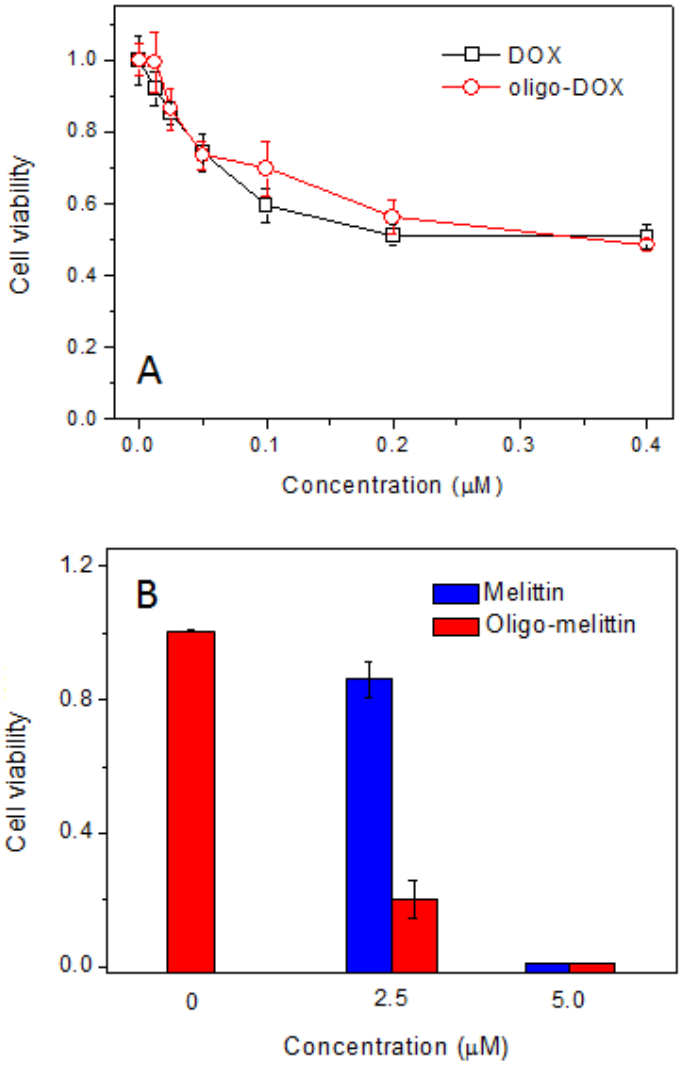

Figure 7. In vitro cytotoxicity of (A) DOX- and (B) melittin-loaded oligopeptide-alginate nanoparticles (oligo-DOX, oligo-Melittin) toward Caco-2 cell lines.

4. Conclusions

Melittin-targeting drug carrier, which possesses oligopeptide side chain, was synthesized by amidation reaction of sodium alginate with oligopeptide at different oligopeptide:alginate ratios. Alginate and oligopeptide-alginate nanoparticles were prepared by adding $CaCl_2$. The introduction of oligopeptide side chain on alginate had a beneficial effect on the size control of nanoparticles: The average size of alginate nanoparticles decreased about 1/4 after the 10 % substitution of carboxylate moiety in alginate to oligopeptide, indicating the interaction between oligopeptide. The ability of hydrogen bonding interaction may exert on the interaction with melittin, which is essentially amphiphilic peptide. In fact, the melittin loading was more superior in oligopeptide-alginate nanoparticle than in alginate nanoparticle, in contrast to the fact of similar DOX loading on both nanoparticles. Moreover, the viability examination also showed the excellent effectiveness of melittin-loaded oligopeptide-alginate nanoparticles in comparison with free melittin. This investigation demonstrates the advantage of oligopeptide-alginate nanoparticles as a melittin carrier and also the possibility of their usage as a carrier for peptide-based drugs.

References

[1]. Ferlay, J.; Soerjomataram, I.; Ervik, M.; Dikshit, R.; Eser, S.; Mathers, C.; Rebelo, M.P.D.; Forman, D.; Bray, F. GLOBOCAN2012v1.0, cancer incidence and mortality worldwide: IARC cancerbase. No.11 [Internet]. Lyon, France. Int. Agency Res. Cancer. 2013; **11**. http://globocan.iarc.f

[2]. Danhier, F.; Preat, V. Strategies to improve the EPR effect for the delivery of anti-cancer nanomedicines. Cancer Cell Microenvi. 2 (2015), 1-7.

[3]. Cho, K.; Wang, X.; Nie, S.; Chen, Z.G.; Shin, D.M. Therapeutic nanoparticles for drug delivery in cancer. Clin. Cancer Res. 14 (2008), 1310-1316.

[4]. Soni, G.; Yadav, K.S. Applications of nanoparticles in treatment and diagnosis of leukemia. Mater. Sci. Eng. C. Mater. Biol. Appl. 47 (2015), 156-164.

[5]. Masood, F. Polymeric nanoparticles for targeted drug delivery system for cancer therapy. Mater. Sci. Eng: C. 60 (2016), 569-578.

[6]. Wang, A.Z.; Langer, R.; Farokhzad, O.C. Nanoparticle delivery and cancer drugs. Annu. Rev. Med. 63 (2012), 185-198.

[7]. Hu, C.M.J.; Zhang, L. Nanoparticle-based combination therapy toward overcoming drug resistance in cancer. Biochem. Pharm. 83 (2012), 1104-1111.

[8]. Mora-Huertas, C.E.; Garrigues, O.; Fessi, H.; Elaissari, A. Nanocapsules prepared via nanoprecipitation and emulsification-diffusion methods: comparative study Eur. J. Pharm. Biopharm. 80 (2012), 235-239.

[9]. Liu, Y.; Wang, W.; Yang, J.; Zhou, C.; Sun, J. pH-sensitive polymeric micelles triggered drug release for extracellular and intracellular drug targeting delivery. Asian J. Pharm. Sci. 8 (2013), 159-167.

[10]. Agarwal, T.; Gautham, S.N.; Narayana, H.; Pal, K.; Pramanik, K.; Giri, S., Banerjee, I. Calcium alginate-carboxymethyl cellulose beads for colon-targeted drug delivery. Inter. J. Bio. Macro. 75 (2015) 409-417.

[11]. Jo, M.; Park, M.H.; Kollipara, P.S.; Jun An, B.; Song, H.S.; Han, S.B.; Kim, J.H.; Song, M.J.; Hong, J.T. Anti-cancer effect of bee venom toxin and melittin in ovarian cancer cells through induction of death receptors and inhibition of JAK2/STAT3 pathway. Toxic. Appl. Pharm. 258 (2012) 72-81.

[12]. Liu, C.C.; Hau, D.J.; Zhang, Q.; An, J.; Zhao, J.J.; Chen, B.; Zhang, L.L; Yang, H. Application of bee venom and its main constituent melittin for cancer treatment. Cancer. Chemother. Pharmacol. 78 (2016) 1113-1130.

[13]. Huh, J.E.; Baek, Y.H.; Lee, M.H.; Choi, D.Y.; Park, D.S.; Lee, J.D. Bee venom inhibits tumor angiogenesis and metastasis by inhibiting tyrosine phosphorylation of VEGFR-2 in LL-tumor-bearing mice. Cancer Lett. 292 (2010) 98-110.

[14]. Gajski, G.; Garaj-Vrhovac, V. Melittin : a lytic peptide with anticancer properties. Environ. Toxic. Pharm. 36 (2013) 697-705.

[15]. Gao, J.; Xie, C.; Zhang, M.; Wei, M.; Yan, Z.; Ren, Y.; Ying, M.; Lu, W. RGD-modified lipid disks as drug carriers for tumor targeted drug delivery. Nanoscale. 8 (2016) 7209-7216.

[16]. Leifer, A., Lippincott, E.R. The infrared spectra of some amino acids. J. Am. Chem. Soc. 79 (1957) 5098-5101.

[17]. Imae, T.; Ikeda, S. Infrared Spectra and Conformation of Monodisperse Oligo-γ-Benzyl-L-Glutamates in Solution. Biopolymers, 23 (1984) 2573-2586.

[18]. Venyaminov, S.Y.; Kalnin, N.N. Quantitative IR spectrophometry of peptide compounds in water solutions. I. spectral parameters of amine acid residue absorption bands. Biopolym. 30 (1990) 1243-1257.

[19]. Bakker, J.M., Aleese, L.M., Meijer, G. von Helden, G. Fingerprint IR spectroscopy to probe amino acid conformations in the gas phase. Phys. Rev. Lett. 91 (2003) 2030031-2030034.

[20]. Ito, M.; Imae, T.; Aoi, K.; Tsutsumiuchi, K.; Noda, H.; Okada, M. In Situ Investigation of Adlayer Formation and Adsorption Kinetics of Amphiphilic Surface-Block Dendrimers on Solid Substrates, Langmuir, 18 (2002) 9757-9764.

[21]. Ito, M.; Imae, T. Self-assembled Monolayer of Carboxyl-terminated Poly(amido amine) Dendrimer, J. Nanosci. Nanotech., 6 (2006) 1667-1672.

[22]. Yang, J.S.; Ren, H.B.; Xie, Y.J. Synthesis of amidic alginate derivatives and their application in microencapsulation of λ-Cyhalothrin. Biomacromolecules. 12 (2011) 2982-2987.

[23]. Mitamura, K.; Imae, T.; Saito N.; Takai, O. Fabrication and Structure of Alginate Gel Incorporating Gold Nanorods, J. Phys. Chem. 112 (2008) 416-422.

[24]. Azevedo, M.A.; Bourbon, A.I.; Vicente, A.A.; Cerqueira, M.A. Alginate/chitosan nanoparticles for encapsulation and controlled release of vitamin B_2. International. J. Biological Macro. 71 (2014) 141-146.

[25] Imae, T.; Okahashi, K.; Ikeda, S. Structure of Micelles formed by Monodisperse Hexa-(γ-benzyl-L-glutamate) in Solution, Biopolymers, 20 (1981) 2553-2566.

[26] Imae, T.; Ikeda, S. Proton Magnetic Resonance Studies on Conformation and Association of Oligo-γ-benzyl-L-glutamates in Solution, Biopolymers, 24 (1985) 2381-2402.

[27]. Xie, H.G.; Li, X.X.; Lv, G.J.; Xie, W.Y.; Zhu, J.; Luxbacher, T.; Ma, R.; Ma, X.J. Effect of

surface wettability and charge on protein adsorption onto implantable alginate-chitosan-alginate microcapsule surfaces. J. Biomedical Materials Research. 92A (2010) 1357-1365.
[28]. Matai, I.; Gopinath, P. Chemically cross-linked hybrid nanogels of alginate and PAMAM dendrimer as efficient anticancer drug delivery vehicles. Biomater. Sci. Eng. 2 (2016) 213-223.
[29]. Kayal, S.; Ramanujan, R.V. Doxorubicin loaded PVA coated iron oxide nanoparticles for targeted drug delivery. Mater. Sci. Eng: C. 30 (2010) 484-490.

106年度專題研究計畫成果彙整表

計畫主持人：朱智謙	**計畫編號：**106-2113-M-040-001-
計畫名稱：具有缺氧標靶特性的光控藥物傳遞系統的開發與其在癌球幹細胞的偵測與治療上的應用	

成果項目					量化	單位	質化 （說明：各成果項目請附佐證資料或細項說明，如期刊名稱、年份、卷期、起訖頁數、證號...等）
國內	學術性論文	期刊論文			0	篇	
		研討會論文			4		2018化學年會(詳見C302表)
		專書			0	本	
		專書論文			0	章	
		技術報告			0	篇	
		其他			0	篇	
	智慧財產權及成果	專利權	發明專利	申請中	0	件	
				已獲得	0		
			新型/設計專利		0		
		商標權			0		
		營業秘密			0		
		積體電路電路布局權			0		
		著作權			0		
		品種權			0		
		其他			0		
	技術移轉	件數			0	件	
		收入			0	千元	
國外	學術性論文	期刊論文			1	篇	已發表學術論文一篇 DOI: 10.1016/j.colsurfb.2018.12.018
		研討會論文			0		
		專書			0	本	
		專書論文			0	章	
		技術報告			0	篇	
		其他			2	篇	投稿中學術論文2篇。
	智慧財產權及成果	專利權	發明專利	申請中	0	件	
				已獲得	1		國別:美國、申請號:15/358,990、申請日:2016-11-22。 108年3月5日通過，後續取證程序進行中。
			新型/設計專利		0		
		商標權			0		
		營業秘密			0		
		積體電路電路布局權			0		

		著作權	0		
		品種權	0		
		其他	0		
	技術移轉	件數	0	件	
		收入	0	千元	
參與計畫人力	本國籍	大專生	3	人次	大學部專題生：大四兩名、大二一名。
		碩士生	2		碩士生：2名
		博士生	0		
		博士後研究員	0		
		專任助理	0		
	非本國籍	大專生	0		
		碩士生	0		
		博士生	0		
		博士後研究員	0		
		專任助理	0		
其他成果 （無法以量化表達之成果如辦理學術活動、獲得獎項、重要國際合作、研究成果國際影響力及其他協助產業技術發展之具體效益事項等，請以文字敘述填列。）					

科技部補助專題研究計畫成果自評表

請就研究內容與原計畫相符程度、達成預期目標情況、研究成果之學術或應用價值（簡要敘述成果所代表之意義、價值、影響或進一步發展之可能性）、是否適合在學術期刊發表或申請專利、主要發現（簡要敘述成果是否具有政策應用參考價值及具影響公共利益之重大發現）或其他有關價值等，作一綜合評估。

1. 請就研究內容與原計畫相符程度、達成預期目標情況作一綜合評估
   ■達成目標
   □未達成目標（請說明，以100字為限）
   　□實驗失敗
   　□因故實驗中斷
   　□其他原因
   說明：

2. 研究成果在學術期刊發表或申請專利等情形（請於其他欄註明專利及技轉之證號、合約、申請及洽談等詳細資訊）
   論文：■已發表　□未發表之文稿　□撰寫中　□無
   專利：■已獲得　□申請中　□無
   技轉：□已技轉　□洽談中　■無
   其他：（以200字為限）

3. 請依學術成就、技術創新、社會影響等方面，評估研究成果之學術或應用價值（簡要敘述成果所代表之意義、價值、影響或進一步發展之可能性，以500字為限）
   「光」在應用上具有安全、穩定且易取得之特色，因其波長與強度的高度調節性，而且可以避免侵入式治療，因而衍生出高度醫療應用價值。本計畫所開發之光觸發藥物傳遞系統，就是一種以光照來驅動藥物分子控制釋放的概念。隨著雷射技術的開發，我們可利用高強度的脈衝雷射搭配光纖折疊應用，精準地將藥物分子在指定時間釋放於患部，大幅提升藥物分子的效率。另外，我們也在複合系統中引入癌症標靶特性，提高藥物傳遞的精準性。本研究之價值主要在於所開發出來的材料具有推廣至臨床癌症治療上的潛力。

4. 主要發現
   本研究具有政策應用參考價值：■否　□是，建議提供機關
   （勾選「是」者，請列舉建議可提供施政參考之業務主管機關）
   本研究具影響公共利益之重大發現：□否　□是
   說明：（以150字為限）